

Deep Metric Learning with Chance Constraints

Yeti Z. Gürbüz, *Member, IEEE*, Oğul Can, *Member, IEEE*, A. Aydın Alatan, *Senior, IEEE*

Abstract— Deep metric learning (DML) aims to minimize empirical expected loss of the pairwise intra-/inter- class proximity violations in the embedding image. We relate DML to feasibility problem of finite chance constraints. We show that minimizer of proxy-based DML satisfies certain chance constraints, and that the worst case generalization performance of the proxy-based methods can be characterized by the radius of the smallest ball around a class proxy to cover the entire domain of the corresponding class samples, suggesting multiple proxies per class helps performance. To provide a scalable algorithm as well as exploiting more proxies, we consider the chance constraints implied by the minimizers of proxy-based DML instances and reformulate DML as finding a feasible point in intersection of such constraints, resulting in a problem to be approximately solved by iterative projections. Simply put, we repeatedly train a regularized proxy-based loss and re-initialize the proxies with the embeddings of the deliberately selected new samples. We apply our method with the well-accepted losses and evaluate on four popular benchmark datasets for image retrieval. Outperforming state-of-the-art, our method consistently improves the performance of the applied losses. Code is available at: CCP-DML Framework

Index Terms—Metric learning, chance constraint.

I. INTRODUCTION

DEEP metric learning (DML) poses distance metric problem as learning the parameters of an embedding function so that the semantically similar samples are embedded to the small vicinity in the representation space as the dissimilar ones are placed relatively apart in the Euclidean sense. The typical embedding function is implemented as convolutional neural networks (CNN) for visual tasks and the parameters are learned through minimizing the empirical expected loss with possibly deliberately selected mini-batch gradient updates [1], [2]. The loss terms in the empirical loss penalize violations of the desired intra- and inter-class proximity constraints. Large-scale problems (in terms of $\#classes$) suffer from the noisy estimation of the expected loss with mini-batches [2]–[4]. Recently, augmenting the mini-batches with virtual embeddings called *proxies* is shown to better approximate empirical loss in large-scale problems [2], [4] owing to pseudo-global consideration of the dataset during loss computation. These advances raise a critical question: “How does increasing proxies help?” which is partially addressed empirically with the methods exploiting multiple proxies per class [4]–[6].

Characterizing generalization performance of proxy-based DML can be a decisive step towards theoretically addressing that question. To this end, we approach DML

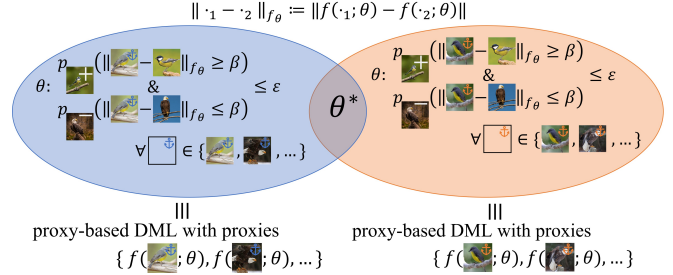


Fig. 1: Simple illustration of our chance constrained DML formulation over two sets where each set’s elements are the embedding function parameters, *i.e.*, θ , that yield an embedding space in which the distances to anchor samples assess the semantic dissimilarity with high probability (*i.e.*, satisfying chance constraints). We consider the parameters of the desired embedding function, *i.e.*, $f(\cdot; \theta^*)$, to lie in the intersection of such sets. We show that to each such set, there corresponds a proxy-based DML solution. Hence, we solve DML as a set intersection problem via solving multiple proxy-based DML problems.

differently by posing it as a feasibility problem. In particular, we consider a chance constraint for desired embedding function and relate it to the typical expected loss of DML. Using such a relation, we provide an upper bound to the generalization error of proxy-based DML. Aligned with the literature, the form of the bound suggests possible room for the improvement on the generalization performance if more and diverse proxies are considered per class. However, straightforward increase of the proxies may not help; since, *i*) proxies of the same class tend to merge [5] and *ii*) memory is prohibitive to arbitrarily increase the proxies.

To alleviate these limitations, we relate minimizer of the proxy-based DML to a feasible point of some chance constraints, and reformulate DML as finding a point at the intersection of the sets that the proxies imply. We provide a scalable algorithm using iterative projections to the individual sets to solve the problem. Each projection corresponds to a regularized proxy-based DML. Hence, we inherently increase the number of diverse proxies included in the problem. We empirically study the implications of our formulation. Evaluation of our method on image retrieval shows state-of-the-art (SOTA) performance in improving the baselines.

II. RELATED WORK

We discuss the works which are most related to ours. Briefly, our contributions include that *i*) we reformulate

DML as a chance constrained feasibility problem, *ii*) we expand on the discussions of the works on the generalization bounds to characterize generalization of proxy-based DML as well as to formally write the feasibility problem as a set intersection to be solved by iterative projections, *iii*) we implicitly utilize arbitrary number of proxies per class.

DML. Most of the existing efforts follow tailoring the loss terms [1], [2] to impose the desired intra- and inter-class proximity constraints in the representation space. Mini-batch construction for empirical estimation of the expected loss is tackled with either *i*) mining of samples in global [7]–[9] and local [3], [10]–[14] manner or *ii*) generating informative samples [15]–[21]. Regularization terms to improve gradient updates towards better generalization are introduced [?], [22], [23]. More sophisticated tracks to enhance the diversity of the semantics embedded to the vector representations involve ensemble [24]–[28] and discriminative feature [17], [29]–[35] learning.

Ranking losses in DML. Typical DML objective enforces distance ranking constraints among the samples in the embedding space via hinge losses penalizing ranking violations. The contrastive [36], [37], triplet [3], [38], and generalized contrastive with margin [12] losses are the simplest forms of the pairwise distance ranking based losses. Proceeding approaches utilize smoothed versions of these losses by replacing hinge loss with log-sum-exp [14] or soft-max [10], [39] expressions. Similarly, mining for tuples [3], [10], [12] and ranking among more samples via soft-batch-mining [10], [13], [39]–[42] are addressed to exploit in-batch tuples with non-trivial settings. In our work, we do not consider crafting a loss term. We rather relate minimizing the ranking losses to feasibility of some chance constraints on the probability of observing pairs violating desired intra-/inter-class distances.

Proxy-based DML. Proxy-based methods consider augmenting the mini-batch with more samples for less noisy estimate of the expected loss and circumvent the costly embedding computation to include more samples in the mini-batches. Proxies typically are vectors representing embeddings of the class centers [42]–[45] and are trained along with the embedding function parameters. Non-trainable proxies are also exploited in [4] to gradually augment mini-batch with previously computed embeddings. In proxy-based DML, the pairwise distances are computed between the proxies and the mini-batch samples. Thus, pseudo-global dataset geometry is considered during loss computation. To better represent global geometry, multiple proxies per class are considered in [5], [6], [46] where the former two build on improving P@1¹ by fine-grained clustering of class samples to overlook intra-class variances. In our analysis, we also align with increasing the proxies. Our work differs in that *i*) we build on reducing the probability of proximity violations (*i.e.*, improving MAP@R¹) and *ii*) we progressively increase the proxies by relating the proxy-based DML instances.

DML as constrained optimization. Pioneer metric learning approaches [38], [47] consider sample-driven proximity constraints to formulate the problem and exploit alternating projections to perform projected gradient ascent. A concurrent work [48] has been reconsidered sample-driven constraints and reformulated DML as a set intersection until very recently. Sharing the set intersection concept, we approach the problem with a different perspective using chance constraints rather than sample-driven constraints, which enables us to formally develop a method that does not suffer from the poor scalability of exploiting class representatives unlike the method proposed in [48] does. What makes our method unique is the theoretically sound way we connect the proxy and set intersection concepts to arbitrarily increase the number of class representatives exploited in the problem.

Fairness in evaluation. Independent works [1], [2], [49] reveal that conventional training and evaluation procedures in DML may fail to properly assess the true order of performance that the methods bring. The consensus for unbiased comparability is evaluation of the methods with their best version under the same experimental settings unless the compared methods demand any particular architecture or experimental setup. Our empirical study is completely aligned with the literature’s claims for unbiased evaluation of our method.

Characterizing generalization bounds. Notion of robustness in learning algorithms is studied in [50] and generalization error bounds of several techniques are derived accordingly. This study is extended to metric learning setting in [51]. These works study the deviation between the expected loss and the empirical loss over the whole dataset. Differently in [52], deviation between two empirical losses, *core-set loss*, is studied and generalization error is characterized by the core-set loss to formulate an optimization objective for their active learning method. Core-set loss typically measures how much is lost when a subset of the training data is exploited. Generalization bound for metric learning is further studied in [53] to analyze and suggest training strategies. Our work expands on the theories in the aforementioned works to characterize and improve generalization bound for proxy-based DML.

III. NOTATION AND PROBLEM DEFINITION

In typical DML, we consider the set $\mathcal{Z} = \mathcal{X} \times \mathcal{Y}$ with elements $z = (x \in \mathcal{X}, y \in \mathcal{Y})$ where \mathcal{X} is a compact space and $\mathcal{Y} = \{1, \dots, C\}$ is a finite label set. We will use x (or y) to denote data (or label) component of z . We have $p_{\mathcal{Z}}$, an unknown probability distribution over \mathcal{Z} . Indicator of the two samples, z and z' , belonging to the same class is denoted as $\iota_{y,y'} \in \{-1, 1\}$ where $\iota_{y,y'} = 1$ if $y = y'$.

We are interested in finding the parameters, θ , of an embedding function, $f(\cdot; \theta) : \mathcal{X} \rightarrow \mathbb{R}^D$, so that the parametric distance, $\|x - x'\|_{f_\theta} := \|f(x; \theta) - f(x'; \theta)\|_2$, between two samples, $(x, x') \sim p_{\mathcal{X}}$, reflects their semantic dissimilarity. For any pair, $(z, z') \sim p_{\mathcal{Z}}$ and embedding function, $f(\cdot; \theta)$, we associate a loss, $\ell(z, z'; \theta)$, penalizing proximity violations in the embedding image. We omit

¹ P@1 (immediate neighbourhood) and MAP@R (global geometry) are explained in the supplementary material.

f dependency in the ℓ notation for simplicity. We are to consider minimization of the expected loss:

$$\theta^* = \arg \min_{\theta} \mathbb{E}_{z, z' \sim p_Z} [\ell(z, z'; \theta)] \quad (1)$$

In practice, we are given a dataset of n instances sampled *i.i.d.* from \mathcal{Z} as $\{z_i\}_{i \in [n]} \sim p_Z$ where $[n] = \{1, \dots, n\}$, and an algorithm, $\mathcal{A}_{s_1 \times s_2}$, which outputs parameters, θ , minimizing empirical expected loss with a training error, $e(\mathcal{A}_{s_1 \times s_2})$, for a given set of pairs, $\{(z_i, z_j)\}_{i, j \in s_1 \times s_2}$, from the dataset, where $s_k = \{s_k(l) \in [n]\}_{l \in [n_k]} \subseteq [n]$ is a pool of indexes chosen from the dataset, $[n]$. *i.e.*,

$$\mathcal{A}_{s_1 \times s_2} := \arg \min_{\theta} \frac{1}{n_1 n_2} \sum_{i \in [n_1]} \sum_{j \in [n_2]} \ell(z_{s_1(i)}, z_{s_2(j)}; \theta), \quad (2)$$

and we formally define DML as $\mathcal{A}_{[n] \times [n]}$, *i.e.*, minimizing empirical expected loss with all possible pairs. We consider improving the generalization error of $\mathcal{A}_{s_1 \times s_2}$ which is:

$$\mathcal{L}(\mathcal{A}_{s_1 \times s_2}) = \mathbb{E}_{z, z' \sim p_Z} [\ell(z, z'; \mathcal{A}_{s_1 \times s_2})]. \quad (3)$$

IV. METHOD

We will iteratively solve multiple proxy-based DML problems. At each problem, we re-initialize the class proxies by samples from the dataset. We relate the problems by regularizing the learned parameters to be in the close vicinity of the previous ones. In the following sections, we provide theoretical foundation behind the motivation of our method. We defer all the proofs to appendix.

We start with reformulating DML with a chance constraint. We will introduce two propositions that allow us to decompose the chance constraint into finite chance constraints. We also show minimizer of proxy-based DML satisfies some chance constraints. Hence, we link DML to finding a point in the intersection of finite sets, which we solve using iterative projections that correspond to regularized proxy-based DML problem instances.

In the formulations throughout the paper, we rely on Lipschitz continuity of the loss function for which we refer to Lemma 1. Our method builds on improving the generalization performance on training domain. Granted, in DML models, the embedding vector is typically obtained by global average pooling of local CNN features. In that manner, local features can be considered as visual words. Thus, if we consider better generalization in training domain, the semantics captured by the visual words can be transferred to represent the samples from an unseen domain. Besides, our empirical studies support that the implications suggested by the formulations are quite effective.

A. Chance Constrained Formulation of Metric Learning

We consider the solution of the following chance constrained feasibility problem:

$$\min_{\theta} 0^T \theta \text{ s. to } p_{z, z' \sim p_Z} (\iota_{y, y'} (\|x - x'\|_{f_\theta} - \beta) \geq 0) \leq \varepsilon, \quad (4)$$

with some small ε . Namely, we want the probability of observing two samples of the same (different) class being apart (close) more than β in the embedding space being

low. We write that probability as expected violation, $\mathbb{E}_{z, z' \sim p_Z} [\mathbb{1}_{\iota_{y, y'} (\|x - x'\|_{f_\theta} - \beta) \geq 0}]$ where $\mathbb{1}(\cdot)$ being indicator function, and bound it for $\beta \geq \alpha > 0$ as:

$$\begin{aligned} p_{z, z' \sim p_Z} (\iota_{y, y'} (\|x - x'\|_{f_\theta} - \beta) \geq 0) \\ \leq 1/\alpha \mathbb{E}_{z, z' \sim p_Z} [(\iota_{y, y'} (\|x - x'\|_{f_\theta} - \beta) + \alpha)_+], \end{aligned} \quad (5)$$

using Markov's inequality where $(u)_+ = \max\{0, u\}$. Note that to each value of the expectation, $e(\theta)$, there corresponds an $\varepsilon = e(\theta)/\alpha$ which the chance constraint satisfies. Hence, we use the expectation as the surrogate of the penalty term for the chance constraint and can redefine the aforementioned feasibility problem as the expected loss minimization in Eq. (1) with $\ell(z, z'; \theta) = (\iota_{y, y'} (\|x - x'\|_{f_\theta} - \beta) + \alpha)_+$. In particular, we end up with minimization of the expected *generalized contrastive loss* [12].

We now consider the relaxed feasibility problem in which we consider m chance constraints conditioned on given m samples $\mathcal{S} = \{z_i\}_{i \in [m]} \sim p_Z$, say *anchor samples*. In other words, we want to find $\theta \in \mathcal{C}_\mathcal{S}$ where:

$$\mathcal{C}_\mathcal{S} = \{\theta \mid p_{z \sim p_Z} (\iota_{y_i, y} (\|x_i - x\|_{f_\theta} - \beta) \geq 0) \leq \varepsilon, \forall i \in [m]\} \quad (6)$$

Using expectation bounds as in Eq. (5), the unconstrained problem becomes:

$$\theta^* = \arg \min_{\theta} \frac{1}{m} \sum_{i \in [m]} \mathbb{E}_{z \sim p_Z} [\ell(z_i, z; \theta)]. \quad (7)$$

We are particularly interested in the problem of the form in Eq. (7) owing to its relation to proxy-based methods to characterize their generalization. Prior to delving into such a relation, we first bound the deviation from the actual expectation in Eq. (1) when we solve Eq. (7) instead.

Proposition 1. *Given $\mathcal{S} = \{z_i\}_{i \in [m]} \stackrel{i.i.d.}{\sim} p_Z$ such that $\forall k \in \mathcal{Y}$ $\{x_i | y_i = k\}$ is $\delta_\mathcal{S}$ -cover² of \mathcal{X} , $\ell(z, z'; \theta)$ is ζ -Lipschitz in x, x' for all y, y' and θ , and bounded by L ; then with probability at least $1 - \gamma$,*

$$\begin{aligned} \left| \mathbb{E}_{z, z' \sim p_Z} [\ell(z, z'; \theta)] - \frac{1}{m} \sum_{i \in [m]} \mathbb{E}_{z \sim p_Z} [\ell(z_i, z; \theta)] \right| \\ \leq \mathcal{O}(\zeta \delta_\mathcal{S}) + \mathcal{O}(L \sqrt{\log \frac{1}{\gamma}/m}). \end{aligned}$$

Proposition 1 gives an upper bound which is controlled by the diversity of the anchor samples defining the relaxed problem. Theoretically, such a controlled bound allows DML to be formulated as a feasibility problem of finite sets for some accepted error tolerance. In practice, the best we can do is using all the samples in the dataset as the anchor samples when defining $\mathcal{C}_\mathcal{S}$ in Eq. (6). Granted that the minimization of the empirical loss of Eq. (7) boils down to the classical DML in Eq. (2), it has different stochastic optimization procedure. The relaxed problem suggests sampling batch of instances rather than pairs, which yields less noisy gradient estimates with the same batch budget³. This intuitively explains the superior performance of the methods using batches augmented by class proxies, past embeddings or more samples (*i.e.*, larger batches), especially in large-scale problems.

² $\mathcal{S} \subset \mathcal{S}'$ is $\delta_\mathcal{S}$ -cover of \mathcal{S}' if $\forall z' \in \mathcal{S}', \exists z \in \mathcal{S} : \|z - z'\|_2 \leq \delta_\mathcal{S}$.

³Besides intuition, implied by Thm. 3 in [50] and Thm. 1 in [51].

B. Reducing Chance Constraints

The loss terms conditioned on anchor samples in Eq. (7) are computationally prohibitive in large-scale problems. Thus, we are interested in reducing the chance constraints, *i.e.*, anchor samples. To this end, proxy-based methods are quite related in that a proxy-based DML constitutes a superset of the feasible region of the primary DML problem in Eq. (4) as we will show shortly.

Proxy-based methods use parametric vectors, $\{\rho_i\}_{i \in [C]}$, to represent embedding of the class centers and minimize the pair losses with respect to those centers. Formally, given a dataset $\{z_i\}_{i \in [n]} \sim p_Z$, proxy-based methods consider the following problem:

$$\min_{\theta, \rho} \frac{1}{nC} \sum_{i \in [C]} \sum_{j \in [n]} \hat{\ell}(\rho_i, z_j; \theta) \quad (8)$$

where $\hat{\ell}(\rho_i, z_j; \theta)$ is a loss term in which the pairwise distance is computed as $\|\rho_i - f(x_j; \theta)\|_2$. We can associate an algorithm, $\mathcal{A}_{sx[n]}$ defined in Eq. (2), to the minimizer of Eq. (8) with $e(\mathcal{A}_{sx[n]})$ training error where $s = \{s(i) \in [n] \mid f(x_{s(i)}; \mathcal{A}_{sx[n]}) = \rho_i\}_{i \in [C]}$. In other words, to each proxy, we associate a sample whose embedding matches that proxy, assuming such sample exists. Hence, the minimizer of the proxy-based methods can be reformulated as the following feasibility problem with the abuse of notation $p_Z = p_{Z \sim p_Z}$:

$$\min_{\theta} 0^\top \theta \text{ s. to } p_Z(\iota_{i,y}(\|x_{s(i)} - x\|_{f_\theta} - \beta) \geq 0) \leq \varepsilon, \forall i \in [C] \quad (9)$$

where $\varepsilon = \frac{1}{\alpha} \mathcal{L}(\mathcal{A}_{sx[n]})$ from Eq. (5) and $\mathcal{L}(\mathcal{A}_{sx[n]})$ defined in Eq. (3) is shown to be bounded in [51]. Reformulation of proxy-based DML defines the feasibility problem in Eq. (6) with one sample per class.

We now consider more general case where we use m samples per class from the dataset, $\{z_i\}_{i \in [n]} \sim p_Z$, to define the feasibility problem. We have m -many disjoint 1-per-class sets, $s = \cup_{k \in [m]} s_k$, where $s_k = \{s_k(i) \in [n] \mid y_{s_k(i)} = i\}_{i \in [C]}$ with $\cap_{k \in [m]} s_k = \emptyset$. We define the problem as:

$$\min_{\theta \in \cap_k C_{s_k}} 0^\top \theta \text{ where } C_{s_k} = \{\theta \mid \forall i \in [C], p_{Z \sim p_Z}(\iota_{i,y}(\|x_{s_k(i)} - x\|_{f_\theta} - \beta) \geq 0) \leq \varepsilon\} \quad (10)$$

Solving the problem by minimizing the empirical expectation bounds in Eq. (7), we end up with an algorithm $\mathcal{A}_{sx[n]}$ in which we are minimizing expected loss over a subset of all possible pairs. We want to characterize the generalization performance of the algorithm $\mathcal{A}_{sx[n]}$. We consider the following bound from [52] for the generalization error:

$$\begin{aligned} \mathbb{E}_{z, z' \sim p_Z} [\ell(z, z'; \mathcal{A}_{sx[n]})] &\leq \left| \frac{1}{|s|n} \sum_{i,j \in sx[n]} \ell(z_i, z_j; \mathcal{A}_{sx[n]}) \right|_{(\mathcal{L}_1)} \\ &+ \left| \mathbb{E}_{z, z' \sim p_Z} [\ell(z, z'; \mathcal{A}_{sx[n]})] - \frac{1}{n^2} \sum_{i,j \in [n] \times [n]} \ell(z_i, z_j; \mathcal{A}_{sx[n]}) \right|_{(\mathcal{L}_2)} \\ &+ \left| \frac{1}{n^2} \sum_{i,j \in [n] \times [n]} \ell(z_i, z_j; \mathcal{A}_{sx[n]}) - \frac{1}{|s|n} \sum_{i,j \in sx[n]} \ell(z_i, z_j; \mathcal{A}_{sx[n]}) \right|_{(\mathcal{L}_3)} \end{aligned} \quad (11)$$

where the bound is controlled by (\mathcal{L}_1) training loss (*i.e.*, $e(\mathcal{A}_{sx[n]})$), (\mathcal{L}_2) the deviation between expected loss and

empirical loss over all possible pairs, and (\mathcal{L}_3) the deviation between empirical loss over all possible pairs and empirical loss over the subset of pairs defining the algorithm, $\mathcal{A}_{sx[n]}$. It is widely observed that high capacity CNNs can reach very small training error. Moreover, \mathcal{L}_2 is proved to be bounded in [51] and is independent of \mathcal{A} . Thus, \mathcal{L}_3 characterizes the generalization performance of using the subset of pairs over exploiting all possible pairs.

Proposition 2. *Given $\{z_i\}_{i \in [n]} \stackrel{i.i.d.}{\sim} p_Z$ and a set $s \subset [n]$. If $s = \cup_k s'_k$ with s'_k is the δ_s -cover of $\{i \in [n] \mid y_i = k\}$ (*i.e.*, the samples in class k), $\ell(z, z'; \theta)$ is ζ -Lipschitz in x, x' for all y, y' and θ , and bounded by L , $e(\mathcal{A}_{sx[n]})$ training error; then with probability at least $1 - \gamma$ we have:*

$$\begin{aligned} &\left| \frac{1}{n^2} \sum_{i,j \in [n] \times [n]} \ell(z_i, z_j; \mathcal{A}_{sx[n]}) - \frac{1}{|s|n} \sum_{i,j \in sx[n]} \ell(z_i, z_j; \mathcal{A}_{sx[n]}) \right| \\ &\leq \mathcal{O}(\zeta \delta_s) + \mathcal{O}(e(\mathcal{A}_{sx[n]})) + \mathcal{O}(L \sqrt{\frac{\log 1/\gamma}{n}}) \end{aligned}$$

Corollary 2.1. *Generalization of the proxy-based methods can be limited by the maximum of distances between the proxies and the corresponding class samples in the dataset.*

Proposition 2 implies that increasing the number of chance constraints with more anchor samples in the feasible point problem formulation of DML improves the generalization error bound as long as the included samples improve the covering radius of the dataset. In other words, including more anchor samples do not improve the bound unless the covering radius is decreased. Similarly, Corollary 2.1 informally suggests possible improvement on the generalization error bound of the proxy-based methods if we manage to introduce more proxies which are spread over the dataset once trained. In practice introducing more proxies generally does not help the performance; since, they eventually coalesce into a single point [5]. Besides, the computation resource limits the number of proxies to be included in the formulation. In the next section, we develop an approach to alleviate these problems.

Algorithm 1 CCP DML

initialize θ^* randomly, given $\{z_i\}_{i \in [n]} \sim p_Z$ dataset

initialize ρ^* with random samples, set budget b

repeat

$\rho \leftarrow \text{GreedyKCenterProxy}(\rho^*, b, f(\cdot; \theta^*))$

repeat

sample $\{j(i) \in [n]\}_{i \in [m]} \sim [n]$ a batch

$g_\theta \leftarrow -\lambda(\theta^* - \theta) + \nabla_\theta \frac{1}{m|\rho|} \sum_{\rho \in [m]} \ell(\rho_i, z_j; \theta)$

$g_\rho \leftarrow \nabla_\rho \frac{1}{m|\rho|} \sum_{\rho \in [m]} \ell(\rho_i, z_j; \theta)$

$(\theta, \rho) \leftarrow \text{ApplyGradient}(\theta, \rho, g_\theta, g_\rho)$

until convergence

$\theta^* \leftarrow \theta, \rho^* \leftarrow \rho$

until convergence

C. Solving the Feasibility Problem

We now introduce our chance constrained programming (CCP) method, outlined in Algorithm 1, exploiting proxy-based training together with satisfying arbitrarily increased

chance constraints. In short, we repeatedly solve a proxy-DML and improve the solution by re-initializing the proxies with the new samples reducing the covering radius.

We consider the problem in Eq. (10) as finding a point in the intersection of the sets. In particular, given dataset $\{z_i\}_{i \in [n]} \sim p_Z$, we have m many 1-per-class sets, $s_k = \{s_k(i) \in [n] \mid y_{s_k(i)} = i\}_{i \in [C]}$, to define the constraint set as $\mathcal{C}_s = \cap_{k \in [m]} \mathcal{C}_{s_k}$. If the sets were closed and convex, the problem would be solvable by iterative projection methods [54], [55]. Nevertheless, it is not uncommon to perform iterative projection methods to non-convex set intersection problems [56], [57]. Hence, we propose to solve the problem approximately by performing iterative projections onto the feasible sets, \mathcal{C}_{s_k} , defined by s_k . At each iteration, k , we solve the following projection problem given $\theta^{(k-1)}$:

$$\theta^{(k)} = \arg \min_{\theta \in \mathcal{C}_{s_k}} \frac{1}{2} \|\theta^{(k-1)} - \theta\|_2^2 \quad (12)$$

where \mathcal{C}_{s_k} is defined in Eq. (10). Using expectation bounds as the surrogate of the penalty terms for the chance constraints as we do in Sec. IV-A, we have:

$$\theta^{(k)} = \arg \min_{\theta} \frac{\lambda}{2} \|\theta^{(k-1)} - \theta\|_2^2 + \frac{1}{C} \sum_{i \in [C]} \mathbb{E}_{z \sim p_Z} [\ell(z_{s_k(i)}, z; \theta)] \quad (13)$$

where λ is a hyperparameter for the projection regularization. We can minimize the resultant loss by using batch stochastic gradient approaches. However, the batch should be augmented by C many anchor samples to compute the loss, which becomes prohibitive for large-scale problems. To alleviate costly embedding computation of C many samples, we propose to use proxies, ρ_i , in place of the embedding of the samples, $z_{s_k(i)}$. Namely, at each iteration k , we initialize $\rho_i = f(z_{s_k(i)}; \theta^{(k-1)})$ and solve:

$$\theta^{(k)}, \rho^* = \arg \min_{\theta, \rho} \frac{\lambda}{2} \|\theta^{(k-1)} - \theta\|_2^2 + \frac{1}{C} \sum_{i \in [C]} \mathbb{E}_{z \sim p_Z} [\ell(\rho_i, z; \theta)] \quad (14)$$

where the resultant problem we solve at each iteration corresponds to a proxy-based DML. Any pairwise distance based loss can replace $\ell(\cdot)$ with anchor samples being class proxies. Namely, we repurpose existing objectives with a regularization term in an iterative manner. Although we set up the formulation using single proxy per class, multiple proxy extension is straightforward.

Theoretically, we should cycle through the sets until convergence to solve $\theta \in \cap_{k \in [m]} \mathcal{C}_{s_k}$. Thus, we must pick anchor samples for each set to initialize proxies. The updates of the proxies are not guaranteed to mimic the actual updates of the corresponding anchor samples. With that being said, we will still have a solution, as Eq. (9) suggests, to feasibility of some chance constraints as long as the converged proxies, ρ^* , are diverse. We empirically observe that the proxies initialized with diverse samples converge to embedding of distinct samples (Fig. 2). Hence, on one hand, we have solutions to different constraint sets as long as we re-initialize the proxies with new samples and solve proxy-based DML problems. On the other hand, Proposition 2 implies that generalization is

Algorithm 2 Greedy K-Center Proxy

input: proxy set ρ , sampling budget b and $f(\cdot; \theta)$
repeat for each class c
 $s_c \leftarrow \{x_i \mid y_i = c\}_{i \in [b]}$, b -sample-per-class
initialize $r_c \leftarrow \{\}$, $p \leftarrow f(s_c; \theta)$
repeat
 $q \leftarrow \arg \max_{u \in p \setminus r_c} \min_{v \in \rho_c \cup r_c} \|u - v\|_2$
 $r_c \leftarrow \{q\} \cup r_c$
until $|r_c| = |\rho_c|$
return $\cup_c r_c$

improved as long as we end up with converged proxies reducing the covering radius. Therefore, the theory suggests a set intersection mechanism to reduce the covering radius yet allows a greedy algorithm via iterative projections to select (*i.e.*, initialize) the next proxies on the fly instead of explicitly defining the sets we will iterate on. Such a result is useful especially for the cases where the dataset is stochastically extended with random data augmentations which obstruct explicit set forming.

Proxy selection. We can simply use random sampling for anchor samples to initialize proxies since we eventually observe informative samples reducing the covering radius through the iterations. We can as well explicitly mine samples that possibly help with reducing the covering radius. Thus, we also exploit clever selection of proxies as outlined in Algorithm 2. Given a budget, b , we sample b many instances per class and compute their embeddings to form a pool. We then select the samples that reduce the covering radius most once added to proxy set. This selection is equivalent to k-Center problem as formulated in [52]. Such a selection of proxies helps converged proxies to be diverse. $b = 1$ reduces to random sampling. In both, we inherently increase the number of anchor samples defining the problem and hence reducing the covering radius.

Relation to cross-batch-memory (XBM) [4]. XBM stores past embeddings in a queue based memory which dequeues the oldest ones at each iteration to enqueue the latest batch. If the memory is much larger than the batch size and *slow drift* [4] is assumed, the loss terms are conditioned to particular proxies until they are updated. To this end, XBM can be seen as solving alternating problems of proxy-based DML with *fuzzy* boundaries and $\lambda = 0$.

D. Implementation Details

Embedding function. For the embedding function, $f(\cdot; \theta)$, we use CNNs with ReLU activation, max- and average-pooling. In particular, we use ResNetV2-20 [58] for MNIST [59] experiments, and ImageNet [60] pretrained BN-Inception [61] for the rest. We exploit architectures until the output of the global average pooling layer. We add a fully connected layer to the output of the global average pooling layer to obtain the embedding vectors of size 2 (ResNetV2-20) and 128 (BN-Inception). We state the following lemma to prove our loss is Lipschitz continuous:

Lemma 1. *Generalized contrastive loss defined as $\ell(z, z'; \theta) := (\nu_{y,y'}(\|x - x'\|_{f_\theta} - \beta) + \alpha)_+$ is $\sqrt{2}\omega^L$ -Lipschitz in x and x' for all y, y', θ for the embedding function $f(\cdot; \theta)$ being L -layer CNN (with ReLU, max-pool, average-pool) with a fully connected layer at the end, where ω is the maximum sum of the input weights per neuron.*

ω can be made arbitrarily small by using weight regularization, which is commonly used. SOTA methods widely use L2 normalization on the embeddings. For normalization, we apply $\hat{v} = v/\|v\|_2$ if $\|v\|_2 \geq 1$ or no normalization otherwise (i.e., $\hat{v} = v$ if $\|v\|_2 \leq 1$). Unlike L2 normalization, such a transform is Lipschitz continuous, hence so are our loss.

Solving projections. Performing a projection defined in (14) involves a minimization problem. We monitor MAP@R validation accuracy and use early stopping patience of 3 to pass the next projection.

V. EXPERIMENTAL WORK

We examine the effectiveness of the proposed proxy-based DML framework for the image retrieval task. We further perform ablation studies for the implications of our formulation as well as the effects of the hyperparameters. We use our own framework implemented in Tensorflow [62] library in the experiments. Throughout the section, we use CCP to refer our framework.

A. Experimental Setup

We mostly follow the procedures proposed in [2] to provide fair and unbiased evaluation of our method as well as comparisons with the other methods. We provide full detail of our experimental setup in the supplementary material for complete transparency and reproducibility.

Datasets. CUB-200-2011 (CUB) [63], Cars196 [64], In-shop [65], Stanford Online Products (SOP) [40] with [2]’s data augmentation.

Evaluation metrics. Precision at 1 (P@1), precision (P@R) and mean average precision (MAP@R) at R where R is defined for each query and is the total number of true references of the query.

Training. Default Adam [66] optimizer with 10^{-5} learning rate, 10^{-4} weight decay, 32 batch size (4 samples per class), 4-fold: 4 models (1 for each $3/4$ train set partition).

Evaluation. Average performance (128-D) and Ensemble (concatenated) performance (512-D).

Losses with CCP. *C1-CCP*: Contrastive [36], *C2-CCP*: Contrastive with positive margin [12], *MS-CCP*: Multi-similarity (MS) [14], *Triplet-CCP*: Triplet [3].

CCP hyperparameters. $\lambda=2 \cdot 10^{-4}$, 8(4) proxies per class with pool size of 12(7) (i.e., $b=12(7)$ in greedy k-Center method) for CUB and Cars (In-shop and SOP).

Compared methods and fairness. We compare our method against proxy-based SoftTriple [5], ProxyAnchor [42] and ProxyNCA++ [45] methods as well as XBM [4]. We note that like the compared methods, our method’s improvement claims do not demand any particular architecture or experimental setup. Therefore, to evaluate the improvements purely coming from the proposed ideas, we

implemented the best version of the compared methods in our framework and evaluate on the same architecture and experimental settings.

B. Ablation Study

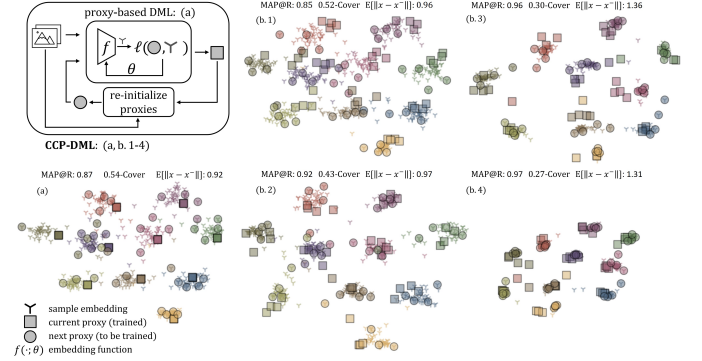


Fig. 2: Illustration^Q of our method (CCP) and the geometry of the embedding space before, (a), and after, (b), our method (through iterations 1-4), where boxes are the converged proxies and the circles are the next proxies as the result of k-Center. In proxy-based DML, proxies are coalesced into one whereas with CCP, we have diverse proxies, resulting reduced covering radius.

Proof of the concept. We evaluate our method on MNIST dataset with 2-D embeddings to show the implications of our formulation. In Fig. 2, we provide the distribution of the samples in the embedding space. We use 4 proxies per class and pool size $b=16$. We observe that when single proxy-based method is converged (Fig. 2-(a)), the class proxies collapse to a single point. Once we continue training with proposed approach (Fig. 2-(b)), the covering radius decreases, leading to performance improvement. It can also be observed that diverse samples results in diverse proxies. We also experiment the case where we use samples instead of proxies. Though it is not practically applicable to large-scale problems, it is important to see whether our intuitions about alternating proxies in place of samples hold. We obtain 98.06% MAP@R performance with sample-based training against 97.21% MAP@R performance of proxy-based training. This empirical result supports our motivation on using the proxies in place of samples. With that being said, it is important to show how such efforts in the training domain are reflected in the test domain. We further provide the visualization of the validation data in CUB dataset in Fig. 10. We compute covering radii for 1 to n sample case in k-Center. Namely, we take k samples with minimum cover for $k \in [n]$ where n is the number of samples per class. We then take the average of these radii to compute a representative metric for the covering radius. We observe that solving single proxy-based DML results in relatively poor generalization in the test domain. On the contrary, solving the problem as the set intersection problem with alternating projections improves the embedding geometry (reduced radius with increased inter-class pairwise distances).

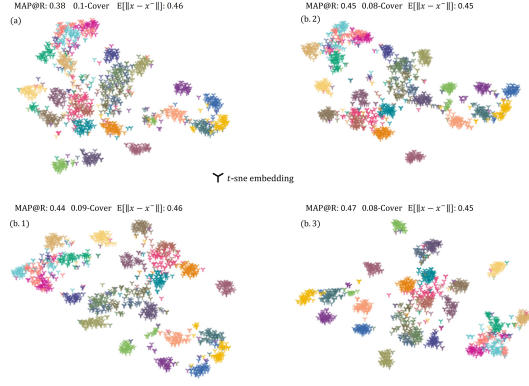


Fig. 3: The geometry of the embedding space \mathcal{Q} before, (a), and after, (b), our method (through iterations 1-3), relating how the generalization efforts in training domain transfer to the geometry of test domain on CUB dataset with C2-CCP. We use 2-D TSNE embeddings of the validation data in the visualization, in which we report MAP@R, average covering radius and average inter-class pairwise distances.

Effect of proxy per class and projection regularization.

We perform Bayesian search on the λ - $\#proxy$ space to see the effect of two in CUB with C2-CCP. We provide the results in Fig. 4. We observe that absence of λ degrades the performance. Similarly, large values of λ causes over-regularization. We obtain interval of $[10^{-1}, 10^{-5}]$ that works well for λ . For the number of proxies, we observe increasing the proxy per class improves performance. On the other hand, the increase saturates as it can also be observed from Fig. 5. As the result of Bayesian parameter search, we take $\lambda=2 \cdot 10^{-4}$ and $\#proxy=8$ with pool size $b=12$ in our evaluations against other methods for CUB and Cars. For SOP and In-shop, we reduce $\#proxy=4$ and $b=7$ owing to relatively less number of samples per class in the dataset.

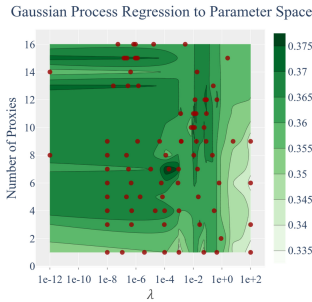


Fig. 4: Bayesian search on λ - $\#proxy$ space

Effect of proxy selection. We perform ablation study with C2-CCP to see the relation between the number of proxies and the pool size used for the proxy selection. We give the corresponding results in Fig. 5. We observe that both increasing the number of proxies and the pool size for proxy selection helps performance. We interestingly see that for single proxy case, increasing the pool size gives no better results than random selection. Owing to our greedy proxy selection, we do consider the past geometry no earlier than single step. Thus, in the single proxy case, we are prone to oscillate between similar samples for proxy selection. On the other hand, selecting the samples that reduce the covering radius most brings better generalization over

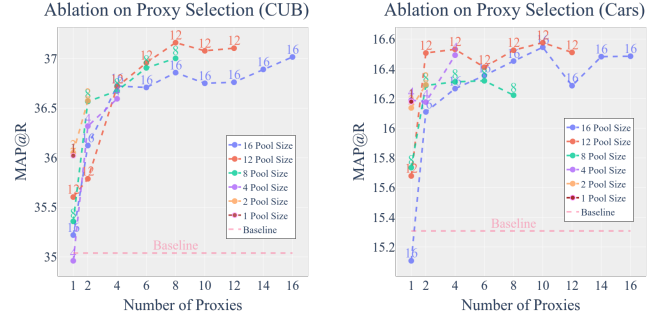


Fig. 5: Analysis of the relation between the number of proxies and the pool size used for the proxy selection on CUB (left) and Cars (right) dataset with C2-CCP.

random selection. With that being said, random sampling in proxy selection (*i.e.*, pool size = $\#proxy$) still works well; since, random sampling indeed can provide diversity in the samples as well. Such a result supports that the key to our method is alternating the proxies with new samples. As long as we re-initialize the proxies with new samples, we will have some diverse proxies through the iterations. To this end, we use Greedy K-Center to pick the samples in a clever way to reduce the covering radius as much as we can (*analogous to mining in batch construction*).

Effect of alternating problems. We provide results on MNIST in Fig. 2 to show the effect of solving alternating problems instead of single proxy-based DML. We additionally evaluate the baseline losses through solving only a single proxy-DML (Loss-Proxy) to show (Fig. 6-(a)) that our performance increase is not solely coming from augmentation of proxies in the problem. We clearly observe that alternating proxies helps performance as our formulation suggests. Moreover, we also provide a typical distribution of the steps per proxy-based projection problem in Fig. 6-(b) to show that we are not greedy on alternating the proxies just to provide more examples. We do have some steps that are relatively low, implying the selected proxies are not informative enough to change the geometry of the embedding space.

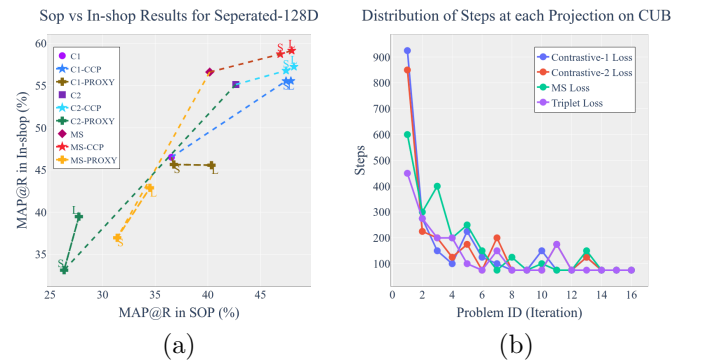


Fig. 6: Impact of alternating proxies (a) and typical distribution of the steps per projection problem (b).

^QMagnified figures are provided in the supplementary material.

Effect of batch size. Batch size plays important role in

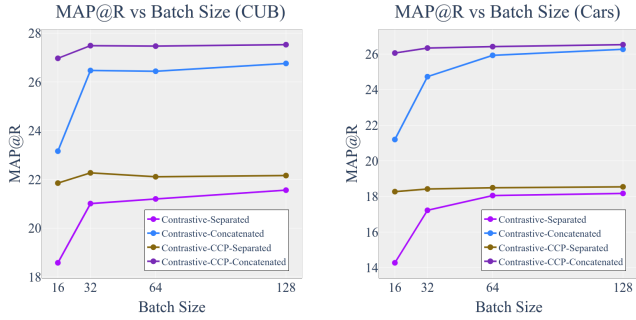


Fig. 7: Analysis of batch size dependence of the performance on CUB (left) and Cars (right) dataset with C2-CCP.

DML methods to perform well. Therefore, we analyze the robustness to the batch size especially for the cases where increasing the batch size is prohibitive. We train baseline contrastive loss and CCP contrastive loss for the batch sizes of 16, 32, 64 and 128. The training setup is the same as in the state-of-the-art comparison (Sec. V-A). In each batch we use 4 samples per class. We provide the results in Fig. 7. We observe that baseline contrastive loss has increasing performance as the batch size increases whereas our method’s performance with small batch size is on par with the large batch size. Thus, our method has reduced batch size complexity.

Computational analysis. Our method outlined in Algorithm 1 puts marginal computation and memory overhead on top of the baseline approaches.

For the computation, we have proxy initialization and weight update steps at the beginning of the each problem instance. In overall, in our system with RTX 2080 Ti GPU and i7 CPU, that additional computation adds on the average 5-10 ms per step (batch update). In particular, for batch size of 32, we typically have rate of 105 ms/batch with Contrastive-CCP whereas vanilla has 97 ms/batch rate. In In-shop and SOP dataset, we have the same rates however for CCP, we have 200 to 400 ms computation overhead due to sampling for proxy initialization. We do not have such overhead in Cars and CUB owing to the much less number of classes. With that being said, we have such 400 ms overhead in In-shop and SOP only at the beginning of new problem instance, which has no significant effect in long run thanks to rather infrequent happening of proxy re-initialization. Due to alternating problems, our method takes more steps to converge than their baseline counterparts. We provide the optimization steps per proxy-based problem instance for several losses in Fig. 6 from which relative convergence can be compared owing

TABLE I: Total steps of training in SOP and In-shop

Method	SOP	In-shop
C2	62K	114K
C2-XBM	81K	93K
C2-CCP	69K	127K
MS	67K	98K
MS-CCP	91K	131K
Triplet	93K	73K
Triplet-CCP	124K	115K
ProxyAnchor	54K	87K
ProxyNCA++	88K	103K
SoftTriple	48K	82K

to each problem instance being a proxy-based method. Nevertheless, we also provide Tab. I to compare the convergence of the methods for SOP and In-shop datasets. The reported numbers are the rounded averages of the 4 models. We observe 10%-35% increase in the optimization steps for the pairwise losses.

For the memory, we store the weights of the previously converged model in the memory as well as the variables for proxies. For the model, approximately 40-45 mb additional GPU memory is used and for the proxies 16.6 mb and 5.9 mb memory is used in SOP and In-shop dataset (75 kb in CUB and Cars).

In summary, CCP brings $\approx 8\%$ increase in back-propagation computation time and only ≈ 60 MB increase in memory for the largest model. CCP takes 10% - 35% more steps to converge than their baseline counterparts due to alternating problems. On the other hand, our method with small batch size performs on par with the large batch size thanks to alternating proxies (Fig. 7). To this manner, marginal increase in computation is seemingly a fair trade-off in improving the performance along with robustness to batch size.

C. Quantitative Results

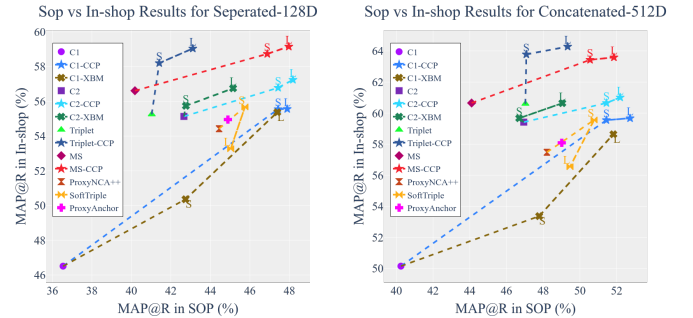


Fig. 8: Summary of relative improvements

We provide quantitative results in Tab. II as well as in Tabs. III and IV for the evaluation of the methods under the same experimental settings and for the conventional evaluation, respectively. We summarize the results in Fig. 8 through average 128-D MAP@R performance of 4-fold models on In-shop and SOP. We use Method-S/L naming convention to denote memory size in XBM, and the proxy per class in SoftTriple and CCP where S denotes 1, and L denotes 4(10) for SoftTriple and 4(8) for CCP in In-shop, SOP (CUB, Cars196). For a fair comparison, we match XBM memory size and the number of proxies in CCP. We observe that CCP consistently outperforms the associated baseline methods on each dataset. Contrastive loss’ great performance with CCP is important to support the implications of our formulation. Furthermore, performance improvements on the loss functions which does not directly fit in our formulation show the broader applicability of our method to the pairwise distance based loss functions. Additionally, the proposed CCP framework outperforms not only the related proxy-based methods but also every

TABLE II: Comparison[†] with the existing methods for the retrieval task on SOP, InShop, CUB, Cars

Method	SOP				In-shop				CUB				Cars196			
	512D		128D		512D		128D		512D		128D		512D		128D	
	P@1	MAP@R	P@1	MAP@R	P@1	MAP@R	P@1	MAP@R	P@1	MAP@R	P@1	MAP@R	P@1	MAP@R	P@1	MAP@R
C1	68.84	40.25	64.96	36.54	80.12	50.15	76.08	46.51	63.67	23.08	56.21	19.06	77.75	23.50	64.17	16.13
C1-XBM-L	78.68	51.82	75.37	47.39	88.39	58.64	85.75	55.37	65.40	24.87	57.57	19.84	83.68	27.93	72.13	18.83
C1-CCP-L	79.53	52.73	76.24	48.07	88.52	59.67	85.50	55.56	68.11	27.11	59.56	21.27	83.76	28.32	72.05	18.96
C2	74.87	46.94	71.15	42.66	86.32	59.42	83.04	55.13	67.49	26.47	59.73	21.01	81.04	24.73	69.17	17.22
C2-XBM-L	76.66	49.04	73.47	45.15	87.66	60.64	84.58	56.75	68.62	26.83	60.18	21.41	82.40	25.99	70.01	18.01
C2-CCP-L	78.95	52.19	75.92	48.18	88.52	61.07	86.11	57.24	69.73	28.02	62.39	22.67	82.89	26.27	72.16	18.52
MS	72.74	44.10	68.96	40.18	88.37	60.65	85.39	56.61	64.65	24.15	57.24	19.64	80.88	26.23	69.27	18.25
MS-CCP-L	78.96	51.85	75.80	47.97	90.24	63.59	87.10	59.15	68.84	27.44	61.10	22.40	86.26	29.14	74.97	19.85
Triplet	75.40	47.03	70.41	41.03	86.71	60.60	82.58	55.25	64.01	23.43	55.51	18.51	78.44	23.11	64.57	15.68
Triplet-CCP-L	77.09	49.33	72.21	43.11	89.44	64.28	86.00	59.04	65.36	24.53	56.65	19.31	81.84	25.21	68.75	17.43
ProxyAnchor	77.10	49.01	73.86	44.89	88.08	58.09	85.87	54.95	68.43	26.53	60.61	21.48	85.29	27.73	75.79	19.56
ProxyNCA++	76.07	48.20	72.89	44.44	87.33	57.48	84.79	54.42	65.48	24.85	58.49	20.96	82.87	26.34	72.45	19.32
SoftTriple-S/L	78.48	50.77	74.66	45.75	88.37	59.56	85.71	55.68	66.12	26.02	57.94	19.86	84.90	27.80	73.16	19.18

TABLE III: Comparison with the existing methods for the retrieval task in conventional experimental settings with BN-Inception backbone. Red: the best. Blue: the second best. Bold: previous SOTA.

Backbone →	BN-Inception-512D			
Dataset →	CUB	Cars196	SOP	In-shop
Method ↓	R@1	R@1	R@1	R@1
SoftTriple-L [5]	65.40	84.50	78.60	-
C1-XBM-L [4]	65.80	82.00	79.50	89.90
ProxyAnchor [42]	68.40	86.10	79.10	91.50
DiVA [32]	66.80	84.10	78.10	-
ProxyFewer [6]	66.60	85.50	78.00	-
Margin-S2SD [34]	68.50	87.30	79.30	-
C1-CCP-L	67.74	83.74	79.86	90.98
C2-CCP-L	69.87	83.90	80.01	91.72
MS-CCP-L	69.09	86.01	79.75	91.84

single benchmarked approaches in [2]. When compared with SoftTriple and XBM (*i.e.*, multiple proxy methods), our method outperforms by large margin especially in the cases where less number of proxies are used (*i.e.*, *method-S* comparisons in Fig. 8). We observe especially in large-scale datasets (SOP & In-shop) that even single proxy per class brings substantial performance improvement with our CCP.

Conventional Evaluation. We additionally follow the relatively old-fashioned conventional procedure [40] for the evaluation of our method. In this manner, we use the whole train split of the dataset for training and the test split to monitor the training as well as evaluation. We use BN-Inception [61] and ResNet50 [58] architectures as the backbones. We use batch size of 128 for BN-Inception and 96 for ResNet50. We follow the same data augmentation and the optimization procedure which are disclosed in Sec. V-A. We provide R@1 results in Tabs. III and IV for the comparison with SOTA. We observe that our method outperforms SOTA in most cases and performs on par with or slightly worse in a few. We should recapitulate that R@1 is a myopic metric to assess the quality of the embedding space geometry and hence, pushing R@1 does not necessarily reflect the true order of the improvements

TABLE IV: Comparison with the existing methods for the retrieval task in conventional experimental settings with ResNet50 backbone. Red: the best. Blue: the second best. Bold: previous SOTA. [†]Results obtained from [35].

Backbone →	ResNet50			
Dataset →	CUB	Cars196	SOP	In-shop
Method ↓	R@1	R@1	R@1	R@1
C1-XBM ¹²⁸ [4]	-	-	80.60	91.30
ProxyAnchor ⁵¹² [42]	69.70	87.70	80.00 [†]	92.10 [†]
DiVA ⁵¹² [32]	69.20	87.60	79.60	-
ProxyNCA++ ⁵¹² [45]	66.30	85.40	80.20	88.60
Margin-S2SD ⁵¹² [34]	69.00	89.50	81.20	-
LIBC ⁵¹² [35]	70.30	88.10	81.40	92.80
ProxyAnchor-DIML ¹²⁸ [33]	66.46	86.13	79.22	-
C1-CCP-L ⁵¹²	69.87	87.12	82.77	92.07
C2-CCP-L ⁵¹²	71.04	85.93	82.34	92.46
MS-CCP-L ⁵¹²	70.37	89.02	82.27	92.71

that the methods bring. As we observe from Tab. II that the methods sharing similar R@1 (*i.e.*, P@1) performances can differ in MAP@R performance relatively more significantly. In that manner, we firmly believe that comparing MAP@R performances instead of R@1 technically sounds more in showing the improvements of our method.

VI. CONCLUSION

We bring a different perspective to DML formulation in terms of chance constraints. Specifically, we formulate the deep metric problem as a chance constrained optimization problem and theoretically showed that a contrastive loss based deep metric learning objective is a surrogate for the chance constraints. We rigorously convert the initial problem formulation into another form enabling expressing the deep metric problem as a set intersection problem. The theory suggests a set intersection mechanism yet allows a greedy algorithm via iterative projections. To this end, we also relate the solution of a proxy-based DML approach to one of the supersets to be intersected to obtain the desired solution. As a result, we formally develop a proxy-based method that inherently considers arbitrary number of proxies for better generalization, realizing the mechanism suggested by the theory with a simple, yet effective, algorithm.

[†]Extended results with P@R are provided in the supp. material.

REFERENCES

- [1] K. Roth, T. Milbich, S. Sinha, P. Gupta, B. Ommer, and J. P. Cohen, “Revisiting training strategies and generalization performance in deep metric learning,” in *International Conference on Machine Learning*. PMLR, 2020, pp. 8242–8252.
- [2] K. Musgrave, S. Belongie, and S.-N. Lim, “A metric learning reality check,” in *European Conference on Computer Vision*. Springer, 2020, pp. 681–699.
- [3] F. Schroff, D. Kalenichenko, and J. Philbin, “Facenet: A unified embedding for face recognition and clustering,” in *Proceedings of the IEEE conference on computer vision and pattern recognition*, 2015, pp. 815–823.
- [4] X. Wang, H. Zhang, W. Huang, and M. R. Scott, “Cross-batch memory for embedding learning,” in *Proceedings of the IEEE/CVF Conference on Computer Vision and Pattern Recognition*, 2020, pp. 6388–6397.
- [5] Q. Qian, L. Shang, B. Sun, J. Hu, H. Li, and R. Jin, “Softtriple loss: Deep metric learning without triplet sampling,” in *The IEEE International Conference on Computer Vision (ICCV)*, October 2019.
- [6] Y. Zhu, M. Yang, C. Deng, and W. Liu, “Fewer is more: A deep graph metric learning perspective using fewer proxies,” *Advances in Neural Information Processing Systems*, vol. 33, pp. 17 792–17 803, 2020.
- [7] B. Harwood, B. Kumar, G. Carneiro, I. Reid, T. Drummond *et al.*, “Smart mining for deep metric learning,” in *Proceedings of the IEEE International Conference on Computer Vision*, 2017, pp. 2821–2829.
- [8] W. Ge, “Deep metric learning with hierarchical triplet loss,” in *Proceedings of the European Conference on Computer Vision (ECCV)*, 2018, pp. 269–285.
- [9] Y. Suh, B. Han, W. Kim, and K. M. Lee, “Stochastic class-based hard example mining for deep metric learning,” in *The IEEE Conference on Computer Vision and Pattern Recognition (CVPR)*, June 2019.
- [10] K. Sohn, “Improved deep metric learning with multi-class n-pair loss objective,” in *Advances in Neural Information Processing Systems*, 2016, pp. 1857–1865.
- [11] Y. Yuan, K. Yang, and C. Zhang, “Hard-aware deeply cascaded embedding,” in *Proceedings of the IEEE international conference on computer vision*, 2017, pp. 814–823.
- [12] C.-Y. Wu, R. Manmatha, A. J. Smola, and P. Krahenbuhl, “Sampling matters in deep embedding learning,” in *Proceedings of the IEEE International Conference on Computer Vision*, 2017, pp. 2840–2848.
- [13] X. Wang, Y. Hua, E. Kodirov, G. Hu, R. Garnier, and N. M. Robertson, “Ranked list loss for deep metric learning,” in *The IEEE Conference on Computer Vision and Pattern Recognition (CVPR)*, June 2019.
- [14] X. Wang, X. Han, W. Huang, D. Dong, and M. R. Scott, “Multi-similarity loss with general pair weighting for deep metric learning,” in *The IEEE Conference on Computer Vision and Pattern Recognition (CVPR)*, June 2019.
- [15] Y. Duan, W. Zheng, X. Lin, J. Lu, and J. Zhou, “Deep adversarial metric learning,” in *Proceedings of the IEEE Conference on Computer Vision and Pattern Recognition*, 2018, pp. 2780–2789.
- [16] Y. Zhao, Z. Jin, G.-j. Qi, H. Lu, and X.-s. Hua, “An adversarial approach to hard triplet generation,” in *Proceedings of the European Conference on Computer Vision (ECCV)*, 2018, pp. 501–517.
- [17] X. Lin, Y. Duan, Q. Dong, J. Lu, and J. Zhou, “Deep variational metric learning,” in *Proceedings of the European Conference on Computer Vision (ECCV)*, 2018, pp. 689–704.
- [18] W. Zheng, Z. Chen, J. Lu, and J. Zhou, “Hardness-aware deep metric learning,” in *The IEEE Conference on Computer Vision and Pattern Recognition (CVPR)*, June 2019.
- [19] B. Ko and G. Gu, “Embedding expansion: Augmentation in embedding space for deep metric learning,” in *Proceedings of the IEEE/CVF Conference on Computer Vision and Pattern Recognition*, 2020, pp. 7255–7264.
- [20] C. Liu, H. Yu, B. Li, Z. Shen, Z. Gao, P. Ren, X. Xie, L. Cui, and C. Miao, “Noise-resistant deep metric learning with ranking-based instance selection,” in *Proceedings of the IEEE/CVF Conference on Computer Vision and Pattern Recognition*, 2021, pp. 6811–6820.
- [21] G. Gu, B. Ko, and H.-G. Kim, “Proxy synthesis: Learning with synthetic classes for deep metric learning,” in *Proceedings of the AAAI Conference on Artificial Intelligence*, vol. 35, no. 2, 2021, pp. 1460–1468.
- [22] D. Zhang, Y. Li, and Z. Zhang, “Deep metric learning with spherical embedding,” *Advances in Neural Information Processing Systems*, vol. 33, 2020.
- [23] B. Chen, W. Deng, B. Wang, and L. Zhang, “Confusion-based metric learning for regularizing zero-shot image retrieval and clustering,” *IEEE Transactions on Neural Networks and Learning Systems*, pp. 1–14, 2022.
- [24] M. Opitz, G. Waltner, H. Possegger, and H. Bischof, “Bier-boosting independent embeddings robustly,” in *Proceedings of the IEEE International Conference on Computer Vision*, 2017, pp. 5189–5198.
- [25] W. Kim, B. Goyal, K. Chawla, J. Lee, and K. Kwon, “Attention-based ensemble for deep metric learning,” in *Proceedings of the European Conference on Computer Vision (ECCV)*, 2018, pp. 736–751.
- [26] H. Xuan, R. Souvenir, and R. Pless, “Deep randomized ensembles for metric learning,” in *Proceedings of the European Conference on Computer Vision (ECCV)*, 2018, pp. 723–734.
- [27] A. Sanakoyeu, V. Tschernezki, U. Buchler, and B. Ommer, “Divide and conquer the embedding space for metric learning,” in *The IEEE Conference on Computer Vision and Pattern Recognition (CVPR)*, June 2019.
- [28] J. Lu, J. Hu, and Y.-P. Tan, “Discriminative deep metric learning for face and kinship verification,” *IEEE Transactions on Image Processing*, vol. 26, no. 9, pp. 4269–4282, 2017.
- [29] K. Roth, B. Brattoli, and B. Ommer, “Mic: Mining interclass characteristics for improved metric learning,” in *The IEEE International Conference on Computer Vision (ICCV)*, October 2019.
- [30] T.-T. Do, T. Tran, I. Reid, V. Kumar, T. Hoang, and G. Carneiro, “A theoretically sound upper bound on the triplet loss for improving the efficiency of deep distance metric learning,” in *The IEEE Conference on Computer Vision and Pattern Recognition (CVPR)*, June 2019.
- [31] P. Jacob, D. Picard, A. Histace, and E. Klein, “Metric learning with horde: High-order regularizer for deep embeddings,” in *The IEEE International Conference on Computer Vision (ICCV)*, October 2019.
- [32] T. Milbich, K. Roth, H. Bharadhwaj, S. Sinha, Y. Bengio, B. Ommer, and J. P. Cohen, “Diva: Diverse visual feature aggregation for deep metric learning,” in *European Conference on Computer Vision*. Springer, 2020, pp. 590–607.
- [33] W. Zhao, Y. Rao, Z. Wang, J. Lu, and J. Zhou, “Towards interpretable deep metric learning with structural matching,” in *Proceedings of the IEEE/CVF International Conference on Computer Vision*, 2021, pp. 9887–9896.
- [34] K. Roth, T. Milbich, B. Ommer, J. P. Cohen, and M. Ghassemi, “S2sd: Simultaneous similarity-based self-distillation for deep metric learning,” in *ICML 2021: 38th International Conference on Machine Learning*, 2021, pp. 9095–9106.
- [35] J. Seidenschwarz, I. Elezi, and L. Leal-Taixé, “Learning intra-batch connections for deep metric learning,” in *Proceedings of the 38th International Conference on Machine Learning, ICML 2021, 18–24 July 2021, Virtual Event*, ser. Proceedings of Machine Learning Research, vol. 139. PMLR, 2021, pp. 9410–9421.
- [36] R. Hadsell, S. Chopra, and Y. LeCun, “Dimensionality reduction by learning an invariant mapping,” in *2006 IEEE Computer Society Conference on Computer Vision and Pattern Recognition (CVPR’06)*, vol. 2. IEEE, 2006, pp. 1735–1742.
- [37] J. Hu, J. Lu, and Y.-P. Tan, “Discriminative deep metric learning for face verification in the wild,” in *Proceedings of the IEEE conference on computer vision and pattern recognition*, 2014, pp. 1875–1882.
- [38] K. Q. Weinberger, J. Blitzer, and L. K. Saul, “Distance metric learning for large margin nearest neighbor classification,” in *Advances in neural information processing systems*, 2006, pp. 1473–1480.
- [39] B. Yu and D. Tao, “Deep metric learning with tuplet margin loss,” in *The IEEE International Conference on Computer Vision (ICCV)*, October 2019.
- [40] H. Oh Song, Y. Xiang, S. Jegelka, and S. Savarese, “Deep metric learning via lifted structured feature embedding,” in

- Proceedings of the IEEE Conference on Computer Vision and Pattern Recognition*, 2016, pp. 4004–4012.
- [41] X. Yang, P. Zhou, and M. Wang, “Person reidentification via structural deep metric learning,” *IEEE Transactions on Neural Networks and Learning Systems*, vol. 30, no. 10, pp. 2987–2998, 2019.
 - [42] S. Kim, D. Kim, M. Cho, and S. Kwak, “Proxy anchor loss for deep metric learning,” in *Proceedings of the IEEE/CVF Conference on Computer Vision and Pattern Recognition*, 2020, pp. 3238–3247.
 - [43] Y. Movshovitz-Attias, A. Toshev, T. K. Leung, S. Ioffe, and S. Singh, “No fuss distance metric learning using proxies,” in *Proceedings of the IEEE International Conference on Computer Vision*, 2017, pp. 360–368.
 - [44] B. Chen, W. Deng, and H. Shen, “Virtual class enhanced discriminative embedding learning,” *Advances in Neural Information Processing Systems*, vol. 31, pp. 1942–1952, 2018.
 - [45] E. W. Teh, T. DeVries, and G. W. Taylor, “Proxynca++: Revisiting and revitalizing proxy neighborhood component analysis,” in *European Conference on Computer Vision (ECCV)*. Springer, 2020.
 - [46] O. Rippel, M. Paluri, P. Dollar, and L. Bourdev, “Metric learning with adaptive density discrimination,” *International Conference on Learning Representations*, 2016.
 - [47] E. P. Xing, M. I. Jordan, S. J. Russell, and A. Y. Ng, “Distance metric learning with application to clustering with side-information,” in *Advances in neural information processing systems*, 2003, pp. 521–528.
 - [48] O. Can, Y. Z. Gürbüz, and A. A. Alatan, “Deep metric learning with alternating projections onto feasible sets,” in *2021 IEEE International Conference on Image Processing (ICIP)*. IEEE, 2021, pp. 1264–1268.
 - [49] I. Fehervari, A. Ravichandran, and S. Appalaraju, “Unbiased evaluation of deep metric learning algorithms,” *arXiv preprint arXiv:1911.12528*, 2019.
 - [50] H. Xu and S. Mannor, “Robustness and generalization,” *Machine learning*, vol. 86, no. 3, pp. 391–423, 2012.
 - [51] A. Bellet and A. Habrard, “Robustness and generalization for metric learning,” *Neurocomputing*, vol. 151, pp. 259–267, 2015.
 - [52] O. Sener and S. Savarese, “Active learning for convolutional neural networks: A core-set approach,” in *International Conference on Learning Representations*, 2018.
 - [53] M. Dong, X. Yang, R. Zhu, Y. Wang, and J. Xue, “Generalization bound of gradient descent for non-convex metric learning,” *Neural Information Processing Systems Foundation*, 2020.
 - [54] L. M. Bregman, “The relaxation method of finding the common point of convex sets and its application to the solution of problems in convex programming,” *USSR computational mathematics and mathematical physics*, vol. 7, no. 3, pp. 200–217, 1967.
 - [55] H. H. Bauschke and A. S. Lewis, “Dykstras algorithm with bregman projections: A convergence proof,” *Optimization*, vol. 48, no. 4, pp. 409–427, 2000.
 - [56] C. Pang, “Nonconvex set intersection problems: From projection methods to the newton method for super-regular sets,” *arXiv preprint arXiv:1506.08246*, 2015.
 - [57] J. Solomon, F. De Goes, G. Peyré, M. Cuturi, A. Butscher, A. Nguyen, T. Du, and L. Guibas, “Convolutional wasserstein distances: Efficient optimal transportation on geometric domains,” *ACM Transactions on Graphics (TOG)*, vol. 34, no. 4, p. 66, 2015.
 - [58] K. He, X. Zhang, S. Ren, and J. Sun, “Identity mappings in deep residual networks,” in *European conference on computer vision*. Springer, 2016, pp. 630–645.
 - [59] Y. LeCun and C. Cortes, “MNIST handwritten digit database,” 2010. [Online]. Available: <http://yann.lecun.com/exdb/mnist/>
 - [60] O. Russakovsky, J. Deng, H. Su, J. Krause, S. Satheesh, S. Ma, Z. Huang, A. Karpathy, A. Khosla, M. Bernstein *et al.*, “Imagenet large scale visual recognition challenge,” *International journal of computer vision*, vol. 115, no. 3, pp. 211–252, 2015.
 - [61] S. Ioffe and C. Szegedy, “Batch normalization: Accelerating deep network training by reducing internal covariate shift,” in *International conference on machine learning*. PMLR, 2015, pp. 448–456.
 - [62] M. Abadi, P. Barham, J. Chen, Z. Chen, A. Davis, J. Dean, M. Devin, S. Ghemawat, G. Irving, M. Isard *et al.*, “Tensorflow: a system for large-scale machine learning,” in *OSDI*, vol. 16, 2016, pp. 265–283.
 - [63] C. Wah, S. Branson, P. Welinder, P. Perona, and S. Belongie, “The caltech-ucsd birds-200-2011 dataset,” 2011.
 - [64] A. Krause and D. Golovin, “Submodular function maximization,” in *Tractability: Practical Approaches to Hard Problems*. Cambridge University Press, 2014, pp. 71–104.
 - [65] Z. Liu, P. Luo, S. Qiu, X. Wang, and X. Tang, “Deepfashion: Powering robust clothes recognition and retrieval with rich annotations,” in *Proceedings of the IEEE conference on computer vision and pattern recognition*, 2016, pp. 1096–1104.
 - [66] D. P. Kingma and J. Ba, “Adam: A method for stochastic optimization,” *arXiv preprint arXiv:1412.6980*, 2014.
 - [67] A. W. Van Der Vaart, A. van der Vaart, A. W. van der Vaart, and J. Wellner, *Weak convergence and empirical processes: with applications to statistics*. Springer Science & Business Media, 2013.
- Yeti Z. Gürbüz** received the B.Sc. and M.Sc. degrees in Electrical and Electronics Engineering Dept. from Middle East Technical University (METU), Ankara, Turkey, in 2011 and 2014, respectively. He was a Research Assistant at Electrical and Electronics Eng. Dept. at METU, Ankara, from 2011 to 2021. He is currently a Ph.D. candidate at Electrical and Electronics Engineering Dept. of METU and researcher at METU Center for Image Analysis, Ankara. His current research interests include machine learning, natural language processing, object recognition and detection.
- Oğul Can** received the B.Sc. degree from Izmir Institute of Technology, Izmir, in 2015 and the M.Sc. degree from Middle East Technical University (METU), Ankara, Turkey, in 2018 in electrical and electronics engineering. He has been researcher at METU Center for Image Analysis, Ankara since 2015. His current research interests include machine learning, natural language processing, object recognition and detection.
- A. Aydın Alatan** received the B.Sc. degree from Middle East Technical University, Ankara, in 1990, the M.Sc. and D.I.C. degrees from the Imperial College of Science, Medicine and Technology, London, U.K., in 1992, and the Ph.D. degree from Bilkent University, Ankara, in 1997, in electrical engineering. He was a Post-Doctoral Research Associate with the Center for Image Processing Research, Rensselaer Polytechnic Institute, Troy, NY, USA, from 1997 to 1998, and the New Jersey Center for Multimedia Research, New Jersey Institute of Technology, Newark, NJ, USA, from 1998 to 2000. In 2000, he joined the faculty of the Department of Electrical and Electronics Engineering at Middle East Technical University. He is the founding director for Center for Image Analysis (OGAM) at METU. Prof. Dr. Alatan is a member of The Science Academy of Turkey.

EMPIRICAL STUDY DETAILS

In the following sections, we explain our empirical study in detail and provide additional experiments on computational analysis.

A. Reproducibility

We provide full detail of our experimental setup and recapitulate the implementation details for the sake of complete transparency and reproducibility. Code is available at: CCP-DML Framework

B. Experimental Setup

Datasets. We perform our experiments on 4 widely-used benchmark datasets: Stanford Online Products (SOP) [40], In-shop [65], Cars196 [64] and, CUB-200-2011 (CUB) [63].

SOP [40] has 22,634 classes with 120,053 product images. The first 11,318 classes (59,551 images) are split for training and the other 11,316 (60,502 images) classes are used for testing.

In-shop has 7,986 classes with 72,712 images. We use 3,997 classes with 25,882 images as the training set. For the evaluation, we use 14,218 images of 3,985 classes as the query and 12,612 images of 3,985 classes as the gallery set.

Cars196 contains 196 classes with 16,185 images. The first 98 classes (8,054 images) are used for training and remaining 98 classes (8,131 images) are reserved for testing.

CUB-200-2011 dataset consists of 200 classes with 11,788 images. The first 100 classes (5,864 images) are split for training, the rest of 100 classes (5,924 images) are used for testing.

Training Splits. We split datasets into disjoint training, validation and test sets according to [2]. In particular, we partition 50%/50% for training and test, and further split training data to 4 partitions where 4 models are to be trained by exploiting $1/4$ as validation while training on $3/4$. For the ablation studies, we split training set into 3 splits instead of 1 and train a single model on the $2/3$ of the set while using $1/3$ for the validation.

Data augmentation follows [2]. During training, we resize each image so that its shorter side has length 256, then make a random crop between 40 and 256, and aspect ratio between $3/4$ and $4/3$. We resize the resultant image to 227×227 and apply random horizontal flip with 50% probability. During evaluation, images are resized to 256 and then center cropped to 227×227 .

Evaluation metrics. We consider precision at 1 ($P@1$), precision ($P@R$) and mean average precision ($MAP@R$) at R where R is defined for each query⁴ and is the total number of true references as the query. Among those, $MAP@R$ performance metric is shown to better reflect the geometry of the embedding space and to be less noisy

as the evaluation metric [2]. Thus, we use $MAP@R$ to monitor training.

$P@1$: Find the nearest reference to the query. The score for that query is 1 if the reference is of the same class, 0 otherwise. Average over all queries gives $P@1$ metric.

$P@R$: For a query, i , find R_i nearest references to the query and let r_i be the number of true references in those R_i -neighbourhood. The score for that query is $P@R_i = r_i/R_i$. Average over all queries gives $P@R$ metric, i.e., $P@R = \frac{1}{n} \sum_{i \in [n]} P@R_i$, where n is the number of queries.

$MAP@R$: For a query, i , we define $MAP@R_i := \frac{1}{R_i} \sum_{i \in [R_i]} P(i)$, where $P(i) = P@i$ if i^{th} retrieval is correct or 0 otherwise. Average over all queries gives $MAP@R$ metric, i.e., $MAP@R = \frac{1}{n} \sum_{i \in [n]} MAP@R_i$, where n is the number of queries.

Training procedure. For the optimization procedure, we use Adam [66] optimizer for mini-batch gradient descent with a mini-batch size of 32 (4 samples per class), 10^{-5} learning rate, 10^{-4} weight decay, default moment parameters, $\beta_1=.9$ and $\beta_2=.99$. We evaluate validation $MAP@R$ for every 25 steps of training in CUB and Cars196, for 250 steps in SOP and In-shop. We stop training if no improvement is observed for 60 steps and recover the parameters with the best validation performance. Following [2], we train 4 models for each $3/4$ partition of the train set. For the ablation studies, we train a single model on the $2/3$ partition.

Embedding vectors. Embedding dimension is fixed to 128. During training and evaluation, the embedding vectors are L2 normalized using the transformation proposed in Section 4.4. We follow the evaluation method proposed in [2] and produce two results: *i*) Average performance (128 dimensional) of 4-fold models and *ii*) Ensemble performance (concatenated 512 dimensional) of 4-fold models where the embedding vector is obtained by concatenated 128D vectors of the individual models before retrieval.

Losses with CCP. We evaluate our method with *C1-CCP*: Contrastive loss [36], *C2-CCP*: Contrastive loss with positive margin [12], *MS-CCP*: Multi-similarity (MS) loss [14], *Triplet-CCP*: Triplet loss [3]. We should note that ProxyAnchor [42] is indeed proxy-based MS loss except for missing a margin term. Similarly, ProxyNCA [45] is $\log \Sigma$ exp-approximation of proxy-based Triplet with hard negative mining and for single proxy case SoftTriple [5] is equivalent to ProxyNCA. Therefore, our experiments cover wide range of the DML losses.

Compared methods. We compare our method against proxy-based SoftTriple [5], ProxyAnchor [42] and ProxyNCA++ [45] methods as well as XBM [4].

Fairness. We note that like the compared methods (i.e., loss functions, proxy-based methods), our method's improvement claims do not demand any particular architecture or experimental setup. Therefore, to evaluate the improvements purely coming from the proposed ideas, we implemented the best version of the compared methods in our framework and evaluate on the same architecture

⁴A query is an image for which similar images are to be retrieved, and the references are the images in the searchable database.

and experimental settings. In this manner, we stick to BN-Inception with global average pooling architecture to directly compare our method with the benchmarked losses in [2]. To eliminate any framework related performance differences, we re-implemented the methods within our framework and produce the consistent results with [2].

Our experimental setting is fair and unbiased; since,

- The compared methods are either invented loss functions or proxy-based approaches, which do not demand a particular setting to show the effectiveness of the proposed ideas.
- We use the same experimental setting for each method (*e.g.* image size, architecture, embedding size, batch size, data augmentation).
- We implement and re-evaluate all the compared methods on our framework (*i.e.*, train and evaluate).
- We reproduce consistent results reported in [2] to eliminate any framework related performance bias.
- We use the same train and test split as the conventional methods, but we do not exploit test data during training. We use $1/4$ split of train data for the validation set.

Hyperparameters. For the hyperparameter selection, we exploit the recent work [2] that has performed parameter search via Bayesian optimization on variety of losses. We further experiment the suggested parameters from the original papers and official implementations. We pick the best performing parameters. We perform no further parameter tuning for the loss parameters when applied to our method to purely examine the effectiveness of our method.

C1: We adopted XBM’s official implementation for fair comparison. We use 0.5 margin for all datasets.

C2: *C2* has two parameters, (m^+, m^-) : positive margin, m^+ , and negative margin. We set (m^+, m^-) to $(0, 0.3841)$, $(0.2652, 0.5409)$, $(0.2858, 0.5130)$, $(0.2858, 0.5130)$ for CUB, Cars196, In-shop and SOP, respectively.

Triplet: We set its margin to 0.0961, 0.1190, 0.0451, 0.0451 for CUB, Cars196, In-shop and SOP, respectively.

MS: *MS* has three parameters (α, β, λ) . We set (α, β, λ) to $(2, 40, 0.5)$, $(14.35, 75.83, 0.66)$, $(8.49, 57.38, 0.41)$, $(2, 40, 0.5)$ for CUB, Cars196, In-shop and SOP, respectively.

ProxyAnchor: We set its two parameters (δ, α) to $(0.1, 32)$ for all datasets. We use 1 sample per class in batch setting (*i.e.*, 32 classes with 1 samples per batch), we perform 1 epoch warm-up training of the embedding layer, and we apply learning rate multiplier of 100 for the proxies during training.

ProxyNCA++: We set its temperature parameter to 0.1 for all datasets. We use 1 sample per class in batch setting (*i.e.*, 32 classes with 1 samples per batch), we perform 1 epoch warm-up training of the embedding layer, and we apply learning rate multiplier of 100 for the proxies during training.

SoftTriple: *SoftTriple* has 4 parameters $(\lambda, \gamma, \tau, \delta)$. We set $(\lambda, \gamma, \tau, \delta)$ to $(20, 0.1, 0.2, 0.01)$, $(17.69, 19.18, 0.0669, 0.3588)$, $(20, 0.1, 0.2, 0.01)$,

$(100, 47.9, 0.2, 0.3145)$ for CUB, Cars196, In-shop and SOP, respectively. We use 1 sample per class in batch setting (*i.e.*, 32 classes with 1 samples per batch), we perform 1 epoch warm-up training of the embedding layer, and we apply learning rate multiplier of 100 for the proxies during training.

XBM: We evaluate XBM with *C1* and *C2*; since, in the original paper, contrastive loss is reported to be the best performing baseline with XBM. We set the memory size of XBM to the total number of proxies (*i.e.*, $proxy_per_class \times \#classes$) to compare the methodology by disentangling the effect of proxy number. With that being said, we also evaluate XBM with the memory sizes suggested in the original paper. In this manner we use two memory sizes for XBM for each dataset: (S, L) where S and L denote the number of batches in the memory. For CUB and Cars196, CCP uses 1(8) proxies per class for $S(L)$. Thus, we set (S, L) to $(3, 25)$ for CUB and Cars196. For In-shop and SOP, CCP uses 1(4) proxies per class for $S(L)$. Thus, we set (S, L) to $(100, 400)$, $(400, 1400)$ for In-shop and SOP, respectively. We perform 1K steps of training with the baseline loss prior to integrate XBM loss in order to ensure *slow drift* assumption.

CCP: For the hyperparameters of our method, we use 8 proxies per class and $\lambda=2 \cdot 10^{-4}$ for CUB and Cars datasets, as the result of the parameter search; and use pool size, $b=12$, for greedy k-Center method. We select pool size based on our empirical studies on the effect pool size and number of proxies. Due to computation limitations, we use 4 proxy per class, $\lambda=2 \cdot 10^{-4}$ and $b=7$ for SOP and In-shop dataset. We perform no warm-up or do not use learning rate multiplier for the proxies.

RESULTS WITH P@R PERFORMANCES

TABLE V: Comparison with the existing methods for the retrieval task on SOP and In-shop. Red: the overall best. Bold: the loss specific best.

Method	SOP						In-shop					
	512D			128D			512D			128D		
	P@1	P@R	MAP@R	P@1	P@R	MAP@R	P@1	P@R	MAP@R	P@1	P@R	MAP@R
C1	68.84	43.28	40.25	64.96	39.68	36.54	80.12	53.11	50.15	76.08	49.61	46.51
C1-XBM-L	78.68	54.66	51.82	75.37	49.95	47.39	88.39	61.33	58.64	85.75	58.13	55.37
C1-CCP-L	79.53	55.11	52.73	76.24	50.07	48.07	88.52	62.54	59.67	85.50	58.51	55.56
C2	74.87	49.88	46.94	71.15	45.77	42.66	86.32	62.36	59.42	83.04	58.27	55.13
C2-XBM-L	76.66	51.91	49.04	73.47	48.18	45.15	87.66	63.50	60.64	84.58	59.78	56.75
C2-CCP-L	78.95	55.01	52.19	75.92	51.14	48.18	88.52	63.94	61.07	86.11	60.16	57.24
MS	72.74	47.07	44.10	68.96	43.25	40.18	88.37	63.53	60.65	85.39	59.65	56.61
MS-CCP-L	78.96	54.71	51.85	75.80	50.48	47.97	90.24	66.31	63.59	87.10	61.74	59.15
Triplet	75.40	50.13	47.03	70.41	44.32	41.03	86.71	63.81	60.60	82.58	58.74	55.25
Triplet-CCP-L	77.09	52.42	49.33	72.21	46.38	43.11	89.44	67.23	64.28	86.00	62.24	59.04
ProxyAnchor	77.10	51.95	49.01	73.86	47.94	44.89	88.08	60.91	58.09	85.87	57.80	54.95
ProxyNCA++	76.07	51.17	48.20	72.89	47.47	44.44	87.33	60.33	57.48	84.79	57.33	54.42
SoftTriple-S	78.48	53.68	50.77	74.66	48.79	45.75	88.37	62.56	59.56	85.71	58.74	55.68

TABLE VI: Comparison with the existing methods for the retrieval task on CUB and Cars196. Red: the overall best. Bold: the loss specific best.

Method	CUB						Cars196					
	512D			128D			512D			128D		
	P@1	P@R	MAP@R	P@1	P@R	MAP@R	P@1	P@R	MAP@R	P@1	P@R	MAP@R
C1	63.67	33.77	23.08	56.21	29.65	19.06	77.75	33.69	23.50	64.17	26.50	16.13
C1-XBM-L	65.40	35.57	24.87	57.57	30.42	19.84	83.68	37.74	27.93	72.13	28.55	18.83
C1-CCP-L	68.11	37.85	27.11	59.56	32.06	21.27	83.76	37.78	28.32	72.05	28.74	18.96
C2	67.49	37.18	26.47	59.73	31.86	21.01	81.04	34.97	24.73	69.17	27.70	17.22
C2-XBM-L	68.62	37.53	26.83	60.18	32.25	21.41	82.40	36.07	25.99	70.01	28.49	18.01
C2-CCP-L	69.73	38.69	28.02	62.39	33.49	22.67	82.89	36.27	26.27	72.16	28.98	18.52
MS	64.65	34.84	24.15	57.24	30.29	19.64	80.88	36.45	26.23	69.27	28.93	18.25
MS-CCP-L	68.84	38.19	27.44	61.10	33.23	22.40	86.26	38.97	29.14	74.97	30.44	19.85
Triplet	64.01	34.55	23.43	55.51	29.38	18.51	78.44	33.83	23.11	64.57	26.52	15.68
Triplet-CCP-L	65.36	35.42	24.53	56.65	30.17	19.31	81.84	35.61	25.21	68.75	28.21	17.43
ProxyAnchor	68.43	37.36	26.53	60.61	32.36	21.48	85.29	37.53	27.73	75.79	29.91	19.56
ProxyNCA++	65.48	35.60	24.85	58.49	31.73	20.96	82.87	36.56	26.34	72.45	29.91	19.32
SoftTriple-L	68.12	36.98	26.02	57.94	30.63	19.86	84.90	37.69	27.80	73.16	29.60	19.18

MAGNIFIED FIGURES

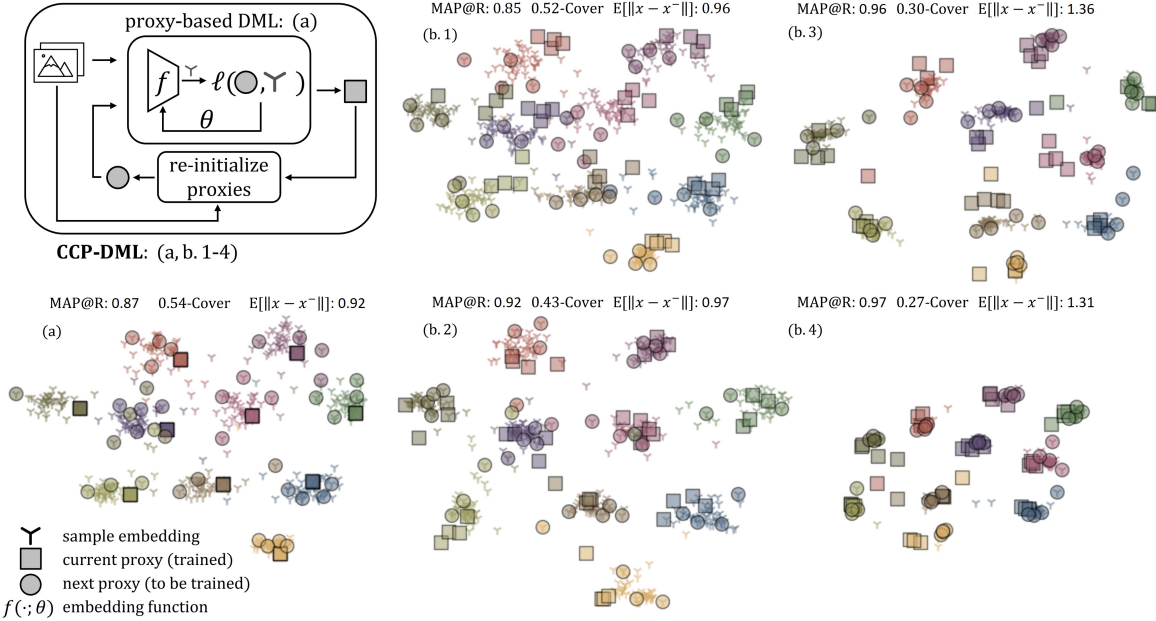


Fig. 9: Illustration of our method and the geometry of the embedding space before, (a), and after, (b), our method (through iterations 1-4), where boxes are the converged proxies and the circles are the next proxies as the result of k-Center. In proxy-based DML, proxies are coalesced into one whereas with CCP, we have diverse proxies, resulting reduced covering radius.

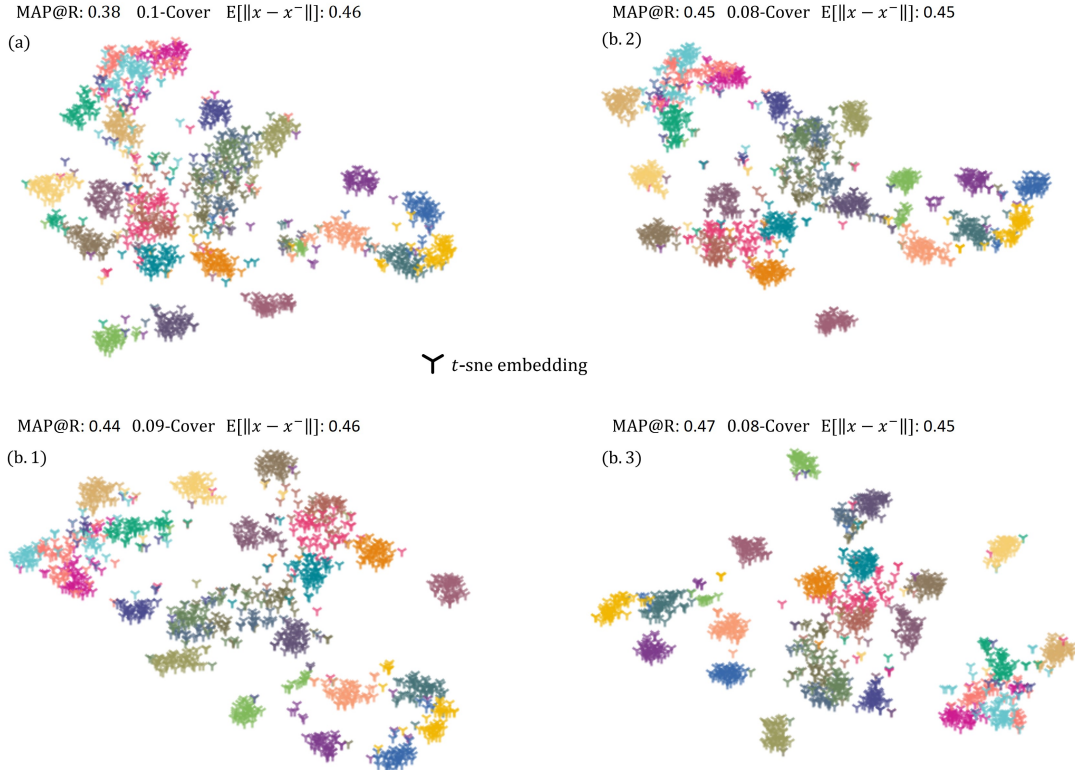


Fig. 10: The geometry of the embedding space before, (a), and after, (b), our method (through iterations 1-3), relating how the generalization efforts in training domain transfer to the geometry of test domain on CUB dataset with C2-CCP. We use 2-D TSNE embeddings of the validation data in the visualization, in which we report MAP@R, average covering radius and average inter-class pairwise distances.

APPENDIX

A. Proof for Lemma 4.1

Lemma 4.1. Generalized contrastive loss defined as $\ell(z, z'; \theta) := (\iota_{y, y'}(\|x - x'\|_{f_\theta} - \beta) + \alpha)_+$ is $\sqrt{2}\omega^L$ -Lipschitz in x and x' for all y, y', θ for the embedding function $f(\cdot; \theta)$ being L -layer CNN (with ReLU, max-pool, average-pool) with a fully connected layer at the end, where ω is the maximum sum of the input weights per neuron.

Proof. We first show that $f(x; \theta)$ is Lipschitz continuous.

We consider $x \in \mathbb{R}^d$ as an input to a layer and $\hat{x} \in \mathbb{R}^{d'}$ as the corresponding output. We express i^{th} component of \hat{x} as $\hat{x}_i = \sum_j w_{i,j} x_{s_i(j)}$ where $s_i = \{s_i(j) \in [d]\}$ is the set of components contributing to \hat{x}_i and $w_{i,j} \in \theta$ is the layer weights. For instance, for a fully connected layer $s_i(j) = j$; for a 3×3 convolutional layer, s_i corresponds to 3×3 window of depth $\#channels$ centered at i . We now consider two inputs x, x' and their outputs \hat{x}, \hat{x}' . We write:

$$\begin{aligned} \frac{\|\hat{x} - \hat{x}'\|_2^2}{\|x - x'\|_2^2} &= \frac{\sum_{i \in [d']} |\hat{x}_i - \hat{x}'_i|^2}{\|x - x'\|_2^2} = \frac{\sum_{i \in [d']} |\sum_j w_{i,j} x_{s_i(j)} - \sum_j w_{i,j} x'_{s_i(j)}|^2}{\|x - x'\|_2^2} \\ &\leq \frac{\sum_{i \in [d']} \sum_j |w_{i,j}|^2 |x_{s_i(j)} - x'_{s_i(j)}|^2}{\|x - x'\|_2^2} \end{aligned}$$

Rearranging terms, we express:

$$\sum_{i \in [d']} \sum_j |w_{i,j}|^2 |x_{s_i(j)} - x'_{s_i(j)}|^2 = \sum_{k \in [d]} \sum_{i,j: s_i(j)=k} |w_{i,j}|^2 |x_k - x'_k|^2$$

If $\sum_{i,j: s_i(j)=k} |w_{i,j}| \leq \omega$ for all k and for all layers, i.e., the absolute sum of the input weights per neuron is bounded by ω , we can write $\sum_{k \in [d]} \sum_{i,j: s_i(j)=k} |w_{i,j}|^2 |x_k - x'_k|^2 \leq \omega^2 \sum_{k \in [d]} |x_k - x'_k|^2 \leq \omega^2 \|x - x'\|_2^2$, hence,

$$\frac{\|\hat{x} - \hat{x}'\|_2}{\|x - x'\|_2} \leq \omega.$$

For max-pooling and average-pooling layers, the inequality holds with $\omega = 1$; since, we can express max-pooling as a convolution where only one weight is 1 and the rest is 0; and similarly, we can express average-pooling as a convolution where the weights sum up to 1.

For ReLU activation, we consider the fact that $|\max\{0, u\} - \max\{0, v\}| \leq |u - v|$ to write:

$$\frac{\|ReLU(x) - ReLU(x')\|_2}{\|x - x'\|_2} \leq 1.$$

Therefore, L -layer CNN $f(x; \theta)$ is ω^L -Lipschitz.

We now consider $\ell(z, z'; \theta) = \max\{0, \iota_{y, y'}(\|f(x; \theta) - f(x'; \theta)\|_2 - \beta) + \alpha\}$ as $g(h(f(x; \theta), f(x'; \theta)))$ where $g(h) = \max\{0, \iota_{y, y'}(h - \beta) + \alpha\}$ is 1-Lipschitz, and $h(f, f') = \|f - f'\|_2$ is $\sqrt{2}$ -Lipschitz and 1-Lipschitz in f for fixed f' . Thus, for y, y', θ fixed, $\ell(z, z'; \theta) := (\iota_{y, y'}(d_f(x, x'; \theta) - \beta) + \alpha)_+$ is ω^L -Lipschitz in x and in x' ; and $\sqrt{2}\omega^L$ -Lipschitz in both, for all y, y', θ . \square

Note that it is easy to show that the normalization proposed in Section 4.4:

$$\hat{v} = \begin{cases} v & \text{for } \|v\|_2 \leq 1 \\ v/\|v\|_2 & \text{for } \|v\|_2 \geq 1 \end{cases}$$

is 2-Lipschitz. Therefore, our loss is still Lipschitz continuous with normalized embeddings in our framework.

B. Proof for Proposition 4.1

Proposition 4.1. Given $\mathcal{S} = \{z_i\}_{i \in [m]} \stackrel{i.i.d.}{\sim} p_{\mathcal{Z}}$ such that $\forall k \in \mathcal{Y} \{x_i | y_i = k\}$ is $\delta_{\mathcal{S}}$ -cover⁵ of \mathcal{X} , $\ell(z, z'; \theta)$ is ζ -Lipschitz in x, x' for all y, y' and θ , and bounded by L ; then with probability at least $1 - \gamma$,

$$\left| \mathbb{E}_{z, z' \sim p_{\mathcal{Z}}} [\ell(z, z'; \theta)] - \frac{1}{m} \sum_{i \in [m]} \mathbb{E}_{z \sim p_{\mathcal{Z}}} [\ell(z_i, z; \theta)] \right| \leq \mathcal{O}(\zeta \delta_{\mathcal{S}}) + \mathcal{O}(L \sqrt{\log \frac{1}{\gamma}/m}).$$

Proof. We start with defining $\hat{\mathcal{L}}(z; \theta) := \mathbb{E}_{z' \sim p_{\mathcal{Z}}} [\ell(z, z'; \theta)]$. Note that

$$\begin{aligned} \|\hat{\mathcal{L}}(z_1; \theta) - \hat{\mathcal{L}}(z_2; \theta)\|_2 &= |\mathbb{E}_{z' \sim p_{\mathcal{Z}}} [\ell(z_1, z'; \theta)] - \mathbb{E}_{z' \sim p_{\mathcal{Z}}} [\ell(z_2, z'; \theta)]| \\ &\leq \mathbb{E}_{z' \sim p_{\mathcal{Z}}} [|\ell(z_1, z'; \theta) - \ell(z_2, z'; \theta)|]. \end{aligned}$$

⁵ $\mathcal{S} \subset \mathcal{S}'$ is $\delta_{\mathcal{S}}$ -cover of \mathcal{S}' if $\forall z' \in \mathcal{S}', \exists z \in \mathcal{S}$ such that $\|z - z'\|_2 \leq \delta_{\mathcal{S}}$.

Therefore, $\ell(z, z'; \theta)$ being ζ -Lipschitz in x for fixed x', y, y' and θ , and bounded by L implies $\hat{\mathcal{L}}(z; \theta)$ is also ζ -Lipschitz in x for all y, θ and bounded by L . Hence, we have

$$|\hat{\mathcal{L}}(z_i; \theta) - \hat{\mathcal{L}}(z; \theta)| \leq \zeta \delta_S \quad \forall z_i, z : z_i \in \mathcal{S}, z \in \mathcal{Z}, \|z_i - z\|_2 \leq \delta_S$$

From Theorem 14 of [50], we can partition \mathcal{Z} into $K = \min_t \{t : t \text{ is } \frac{\delta_S}{2} \text{-cover of } \mathcal{Z}\}$ disjoint sets, denoted as $\{\mathcal{R}_i\}_{i \in [K]}$, such that $\forall i : z_i \in \delta_S$; both z_i, z being $\in \mathcal{R}_i$ implies $|\hat{\mathcal{L}}(z_i; \theta) - \hat{\mathcal{L}}(z; \theta)| \leq \zeta \delta_S$. Hence, from Theorem 3 of [50], with probability at least $1 - \gamma$, we have:

$$\begin{aligned} \left| \mathbb{E}_{z, z' \sim p_Z} [\ell(z, z'; \theta)] - \frac{1}{m} \sum_{i \in [m]} \mathbb{E}_{z \sim p_Z} [\ell(z_i, z; \theta)] \right| &= \left| \mathbb{E}_{z \sim p_Z} [\hat{\mathcal{L}}(z; \theta)] - \frac{1}{m} \sum_{i \in [m]} \hat{\mathcal{L}}(z_i; \theta) \right| \\ &\leq \zeta \delta_S + L \sqrt{\frac{2K \log 2 + 2 \log 1/\gamma}{m}} \end{aligned}$$

Note that K is dependent on δ_S and satisfies $\lim_{m \rightarrow \infty} \frac{K}{m} \rightarrow 0$ ensuring that the right hand side goes to zero as more samples are exploited and the covering radius is improved. Thus, asymptotically the following holds:

$$\mathbb{E}_{z, z' \sim p_Z} [\ell(z, z'; \theta^*)] \leq \mathcal{O}(\delta_S) + \mathcal{O}(\sqrt{\log \frac{1}{\gamma}/m}) \text{ with probability at least } 1 - \gamma.$$

□

C. Proof for Proposition 4.2

Proposition 4.2. *Given $\{z_i\}_{i \in [n]} \stackrel{i.i.d.}{\sim} p_Z$ and a set $s \subset [n]$. If $s = \cup_k s'_k$ with s'_k is the δ_S -cover of $\{i \in [n] \mid y_i = k\}$ (i.e., the samples in class k), $\ell(z, z'; \theta)$ is ζ -Lipschitz in x, x' for all y, y' and θ , and bounded by L , $e(\mathcal{A}_{\text{sx}[n]})$ training error; then with probability at least $1 - \gamma$ we have:*

$$\left| \frac{1}{n^2} \sum_{i, j \in [n] \times [n]} \ell(z_i, z_j; \mathcal{A}_{\text{sx}[n]}) - \frac{1}{|s|n} \sum_{i, j \in \text{sx}[n]} \ell(z_i, z_j; \mathcal{A}_{\text{sx}[n]}) \right| \leq \mathcal{O}(\zeta \delta_S) + \mathcal{O}(e(\mathcal{A}_{\text{sx}[n]})) + \mathcal{O}(L \sqrt{\log \frac{1}{\gamma}/n})$$

Proof. We are given a condition on s that we can partition \mathcal{Z} into $m = |s|$ disjoint sets such that any sample from the dataset $(x_i, c), i \in [n]$, has a corresponding sample from $s, (x'_j, c), j \in s$ within δ_S ball. Thus, we start with partitioning \mathcal{Z} into s disjoint sets as $\mathcal{Z} = \cup_i \mathcal{S}_i$ with $\mathcal{S}_i \cap \mathcal{S}_j = \emptyset, \forall i \neq j$.

We define $\ell_{[n]}(z) = \frac{1}{n} \sum_{i \in [n]} \ell(z, z_i, \mathcal{A}_{\text{sx}[n]})$ and $\ell_s(z) = \frac{1}{m} \sum_{i \in s} \ell(z, z_i, \mathcal{A}_{\text{sx}[n]})$ for the sake of clarity. Hence, we are interested in bounding $|\frac{1}{n} \sum_{i \in [n]} \ell_{[n]}(z_i) - \frac{1}{m} \sum_{i \in s} \ell_{[n]}(z_i)|$. We proceed with using triangle inequality to write:

$$\begin{aligned} \left| \frac{1}{n} \sum_{i \in [n]} \ell_{[n]}(z_i) - \frac{1}{m} \sum_{i \in s} \ell_{[n]}(z_i) \right| &\leq \left| \frac{1}{n} \sum_{i \in [n]} \ell_{[n]}(z_i) - \sum_{i \in s} \frac{n_i}{n} \ell_{[n]}(z_i) \right|^{(T1)} + \left| \sum_{i \in s} \frac{n_i}{n} \ell_{[n]}(z_i) - \frac{1}{m} \sum_{i \in s} \ell_{[n]}(z_i) \right|^{(T2)} \end{aligned}$$

For term (T1) we write:

$$(T1) \leq \frac{1}{n} \sum_{i \in [m]} \sum_{z_j \in \mathcal{S}_i} |\ell_{[n]}(z_{s(i)}) - \ell_{[n]}(z_j)| \stackrel{(1)}{\leq} \zeta \delta_S$$

where in (1), we use ζ -Lipschitz of the loss function and the condition $|z_{s(i)} - z_j| \leq \delta_S, \forall z_j \in \mathcal{S}_i$.

Using triangle inequality, we bound term (T2) as:

$$\begin{aligned} \left| \sum_{i \in s} \frac{n_i}{n} \ell_{[n]}(z_i) - \frac{1}{m} \sum_{i \in s} \ell_{[n]}(z_i) \right| &\leq \left| \mathbb{E}_{z \sim p_Z} [\ell_s(z)] - \mathbb{E}_{z \sim p_Z} [\ell_{[n]}(z)] \right|^{(T2.1)} \\ &+ \left| \mathbb{E}_{z \sim p_Z} [\ell_{[n]}(z)] - \sum_{i \in s} \frac{n_i}{n} \ell_{[n]}(z_i) \right|^{(T2.2)} + \left| \mathbb{E}_{z \sim p_Z} [\ell_s(z)] - \frac{1}{n} \sum_{i \in [n]} \ell_s(z_i) \right|^{(T2.3)} \end{aligned}$$

where we use $\frac{1}{m} \sum_{i \in s} \ell_{[n]}(z_i) = \frac{1}{n} \sum_{i \in [n]} \ell_s(z_i)$ in (T2.3).

For (T2.1) we have:

$$(T2.1) \leq \left| \mathbb{E}_{z \sim p_Z} \left[\frac{1}{m} \sum_{i \in s} \ell(z_i, z) - \frac{1}{n} \sum_{i \in [n]} \ell(z_i, z) \right] \right|$$

where we abuse the notation for the sake of clarity and drop parameter, $\mathcal{A}_{\text{sx}[n]}$, dependency from the loss. Rearranging the terms, we have:

$$(T2.1) \leq \left| \mathbb{E}_{z \sim p_Z} \left[\frac{1}{m} \sum_{i \in [m]} \frac{n-m}{n} \ell(z_{s(i)}, z) \right] \right| + \left| \mathbb{E}_{z \sim p_Z} \left[\frac{1}{n} \sum_{i \in [m]} \sum_{j \in \mathcal{S}_i} \ell(z_{s(i)}, z) - \ell(z_j, z) \right] \right|$$

where similar to (T1), the second summand is upper bounded by $\zeta \delta_s$. Using triangle inequality for the first summand, we write:

$$\left| \mathbb{E}_{z \sim p_Z} \left[\frac{1}{m} \sum_{i \in [m]} \frac{n-m}{n} \ell(z_{s(i)}, z) \right] \right| \leq (T2.3) + e(\mathcal{A}_{\text{sx}[n]})$$

Hence, we have:

$$(T2.1) \leq \zeta \delta_s + (T2.3) + e(\mathcal{A}_{\text{sx}[n]})$$

where from Hoeffding's Bound, $(T2.3) \leq L \sqrt{\log \frac{1}{\gamma} / 2n}$ with probability at least $1 - \gamma$:

Finally, we express (T2.2) as:

$$\begin{aligned} (T2.2) &= \left| \sum_{i \in [m]} \mathbb{E}_{z \sim p_Z} [\ell_{[n]}(z) \mid z \in \mathcal{S}_i] p(z \in \mathcal{S}_i) - \sum_{i \in s} \frac{n_i}{n} \ell_{[n]}(z_i) \right| \\ &\leq \left| \sum_{i \in [m]} \mathbb{E}_{z \sim p_Z} [\ell_{[n]}(z) \mid z \in \mathcal{S}_i] \frac{n_i}{n} - \sum_{i \in s} \frac{n_i}{n} \ell_{[n]}(z_i) \right| \\ &\quad + \left| \sum_{i \in [m]} \mathbb{E}_{z \sim p_Z} [\ell_{[n]}(z) \mid z \in \mathcal{S}_i] p(z \in \mathcal{S}_i) - \sum_{i \in [m]} \mathbb{E}_{z \sim p_Z} [\ell_{[n]}(z) \mid z \in \mathcal{S}_i] \frac{n_i}{n} \right| \end{aligned}$$

Rearranging the terms we have:

$$(T2.2) \leq \sum_{i \in [m]} \frac{n_i}{n} \max_{z \in \mathcal{S}_i} |\ell_{[n]}(z) - \ell_{[n]}(z_{s(i)})| + \max_{z \in \mathcal{Z}} |\ell_{[n]}(z)| \sum_{i \in [m]} \left| \frac{n_i}{n} - p(z \in \mathcal{S}_i) \right|$$

where the first summand is bounded above by $\zeta (\delta_s + \varepsilon(n))$ owing to loss being ζ -Lipschitz. Here, we denote $\varepsilon(n)$ as the covering radius of \mathcal{Z} , *i.e.*, the dataset, $\{x_i, y_i\}_{[n]}$ is $\varepsilon(n)$ -cover of $\mathcal{X} \times \mathcal{Y}$. We note that $(n_i)_{i \in [m]}$ is an *i.i.d.* multinomial random variable with parameters n and $(p_Z(z \in \mathcal{S}_i))_{i \in [m]}$. Thus, by the Breteganolle-Huber-Carol inequality (Proposition A6.6 of [67]), we have :

$$(T2.2) \leq \zeta (\delta_s + \varepsilon(n)) + L \sqrt{\frac{2m \log 2 + 2 \log 1/\gamma}{n}}$$

Finally, with probability at least $1 - \gamma$, we end up with:

$$\left| \frac{1}{n} \sum_{i \in [n]} \ell_{[n]}(z_i) - \frac{1}{m} \sum_{i \in s} \ell_{[n]}(z_i) \right| \leq \zeta (3\delta_s + \varepsilon(n)) + e(\mathcal{A}_{\text{sx}[n]}) + L \left(\sqrt{\log \frac{1}{\gamma} / 2n} + \sqrt{\frac{2m \log 2 + 2 \log 1/\gamma}{n}} \right)$$

□

Corollary 4.2.1. *Generalization performance of the proxy-based methods can be limited by the maximum of distances between the proxies and the corresponding class samples in the dataset.*

Proof. The covering radius for each class subset is the maximum distance between the corresponding class samples and the class proxy. We at least know that the generalization error is bounded above with a term proportional to that distance. □